Z. Phys. C – Particles and Fields 33, 483–503 (1987)

Zeitschrift für Physik C Particles and Fields

Neutrino Production of Dimuons

K. Lang[a], A. Bodek, F. Borcherding[b], N. Giokaris[c], I.E. Stockdale[d]
University of Rochester, Rochester, NY 14627, USA

P. Auchincloss, R. Blair, C. Haber[e], S. Mishra, E. Oltman, M. Ruiz[f], F.J. Sciulli, M. Shaevitz, W.H. Smith, R. Zhu[g]
Columbia University, New York, NY 10027, USA

Y.K. Chu, D.B. MacFarlane[h], R.L. Messner[i], D.B. Novikoff[j], M.V. Purohit[b]
California Institute of Technology, Pasadena, CA 91125, USA

D. Garfinkle, F.S. Merritt, M. Oreglia, P. Reutens
Enrico Fermi Institute and Physics Department, University of Chicago, Chicago, IL 60637, USA

R. Coleman, H.E. Fisk, Y. Fukushima[k], Q. Kerns, B. Jin[g], D. Levinthal[l], T. Kondo[k], W. Marsh, P.A. Rapidis, S. Segler, R. Stefanski, D. Theriot, H.B. White, D. Yovanovitch
Fermi National Accelerator Laboratory, Batavia, IL 60510, USA

O. Fackler[m], K. Jenkins[n]
Rockefeller University, New York, NY 10021, USA

Received 19 September 1986

Abstract. Neutrino interactions with two muons in the final state have been studied using the Fermilab narrow band beam. A sample of 18 ν_μ like sign dimuon events with $P_\mu > 9$ GeV/c yields 6.6 ± 4.8 events after background subtraction and a prompt rate of $(1.0 \pm 0.7) \times 10^{-4}$ per single muon event. The kinematics of these events are compared with those of the non-prompt sources. A total of 437 ν_μ and 31 $\bar{\nu}_\mu$ opposite sign dimuon events with $P_\mu > 4.3$ GeV/c are used to measure the strange quark content of the nucleon: $\kappa = 2s/(\bar{u}+\bar{d}) = 0.52^{+0.17}_{-0.15}$ $\left(\text{or} \quad \eta_s = \frac{2s}{u+d} = 0.075 \pm 0.019\right)$ for $100 < E_\nu < 230$ GeV ($\langle Q^2 \rangle = 23$ GeV^2/c^2) using a charm semileptonic branching ratio of (10.9 ± 1.4)% extracted from measurements in e^+e^- collisions and neutrino emulsion data.

[a] On Leave from Institute of Nuclear Studies, Warsaw, Poland

Present addresses:
[b] Fermilab, Batavia, IL 60510, USA
[c] Rockefeller University, New York, NY 10021, USA
[d] University of Illinois, Urbana, IL 61801, USA
[e] Lawrence Berkeley Lab, Berkeley, CA 94720, USA
[f] University of Florida, Gainesville, FL 32611, USA
[g] Institute for High Energy Physics, Beijing, P.R. China
[h] University of Toronto, Toronto, Ontario, Canada M5S1A7
[i] SLAC, Stanford, CA 94305, USA
[j] Hughes Aircraft Co., El Segundo, CA 90245, USA
[k] National Lab for High Energy Physics, Tsukuba-gun, Ibaraki-ken, 305 Japan
[l] Florida State University, Tallahassee, FL 32306, USA
[m] Lawrence Livermore Lab, Livermore, CA 94550, USA
[n] IBM Thomas J. Watson Research Center, Yorktown Heights, NY 10598, USA

Introduction

We report on an experimental study of neutrino induced interactions with two muons of the same and opposite electric charge in the final state. Of these two classes of events, those with two muons of the same charge are expected to be mostly due to pion and kaon decay in the hadron showers of charged current events. As described below, several previous experiments have observed rates somewhat higher than that expected from the hadron shower back-

ground. Although this prompt signal has not been clearly demonstrated, there is considerable interest in these results since there exists no universally acceptable explanation for an excess of events.

In contrast, the source of events with two muons of the opposite charge is well understood both theoretically and experimentally. This class of events results from reactions that produce a charmed quark, followed by the muonic decay of the charmed particle. The weak decay selection rules restrict these events to always have oppositely charged muons in the final state, with one from the neutrino collision and the other from the charm decay. Since charmed quarks are predominantly produced by valence down quarks and sea strange quarks, a measurement of the strange content of the nucleon can be extracted from the production rate and kinematics of the opposite charge events.

The dimuon data come from two runs with the same detector using the Fermilab narrow band neutrino beam as a neutrino source [1]. The first run (Fermilab experiment 616) took place in 1979 and 1980, with an integrated proton flux of 5.4×10^{18} on the production target. The second run took place in 1982 (Fermilab experiment E701) with a flux of 3.4×10^{18} protons. The neutrino beam [2] was produced by decays of sign and momentum selected ($\Delta P/P = \pm 11\%$) pions and kaons in a 352 m long evacuated decay pipe. Data were taken at 11 sign and momentum settings for secondary hadrons ($+100$, ± 120, ± 140, ± 165, ± 200, ± 250 GeV/c), yielding usable neutrinos and antineutrinos with energies between 30 and 230 GeV.

Apparatus Description

The neutrino detector, shown in Fig. 1, was placed in Lab E, located 1,292 m downstream from the beginning of the decay pipe. The apparatus consisted of a target calorimeter instrumented with liquid scintillation counters and spark chambers, followed by an iron toroidal muon spectrometer. The 690 ton target calorimeter was constructed of 168 3 m × 3 m × 5 cm steel plates, 82 3 m × 3 m liquid scintillation counters (located every 10 cm of steel) and 36 3 m × 3 m spark chambers with magnetostrictive readout (located every 20 cm of steel). The average density of the calorimeter was 4.27 g/cm^3. For the second run of the experiment, only the downstream two-thirds of the target was used. Minimum ionizing muons were used to monitor the counter gains. The hadron response of the calorimeter was calibrated with a hadron beam of known momentum. The rms hadron energy resolution was $0.89\sqrt{E}$ (GeV).

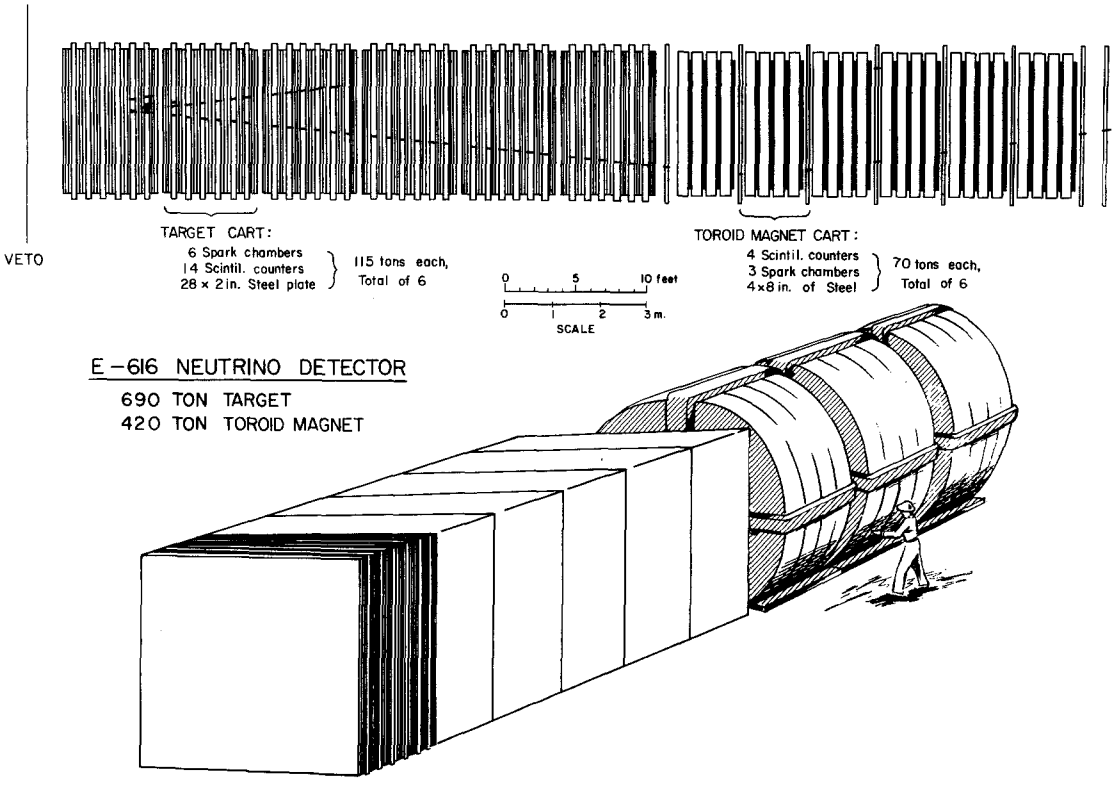

Fig. 1. The CCFRR detector. The steel target region is instrumented with counters and spark chambers to detect the interaction point and to track the muon downstream. The toroids permit measurement of final state muon momenta

The muon spectrometer consisted of three 3 m long iron toroidal magnets (containing 1.6 m of steel each) with 1.8 m outer radius and a 12.7 cm radius hole for the coils. In addition to the gaps between toroids, a gap at the midplane of each toroid was available for instrumentation. In the first run, the five toroid gaps were instrumented with the combination of 1.5 m × 3 m and 3 m × 3 m spark chambers as shown in Fig. 1. In both runs there were 3 m × 3 m spark chambers downstream of the last toroid. In the second run, only the second and fourth gaps were instrumented, each with five 3 m × 3 m spark chambers. The total transverse momentum kick of the toroids was 2.4 GeV/c and the fractional rms momentum resolution was 11%.

Dimuon Analysis

Events with two muons were selected from the entire sample of charged current triggers. The selection procedure searched downstream of the hadron shower for either (1) two or more hits in three out of any four consecutive target or toroid spark chambers, or (2) at least 1.7 times minimum ionizing pulse height in at least eight consecutive target or toroid scintillation counters. These requirements correspond to 1 GeV of observed energy loss in steel for each muon. This computer-selected candidate sample contained one-quarter of the charged current data sample. The selection inefficiency for this sample was measured to be less than 1% by scanning 10% of the total data sample. Events in the computer-selected candidate sample were displayed on a fine resolution graphics terminal. Events in which two tracks were seen in the spark chambers and scintillation counters were selected. The selection inefficiency of this visual scan was also found to be less than 1% by triple scanning 25% of the computer selected sample. The computer reconstruction of each of the 3,208 selected dimuon events was examined by physicists and, if necessary, spark chamber hits were reassigned to the correct tracks and their momenta were recalculated.

Events were separated into those produced by muon neutrinos (or antineutrinos) from pion decay (ν_π) and from kaon decay (ν_K). In a narrow band beam, the neutrino energy and decay angle (and therefore the event radius at the detector) are related by decay kinematics. Events due to ν_K and ν_π were distinguished by comparing the energy expected from the transverse radial position of the interaction and the measured total energy. Once this separation was made, the event transverse vertex position determined the incident neutrino energy for ν_K events with a precision of about 10%. The neutrino energy was thus determined independently, from both the event vertex radius and total measured energy.

Dimuon and single muon events passed the same analysis cuts. Events were required to have a transverse vertex within a 2.5 m × 2.5 m square and a longitudinal vertex at least 3.8 m (1.9 m of iron) upstream of the downstream end of the target. These cuts ensured containment of the hadron shower in the target calorimeter. The ν_π event vertex was required to have a transverse radius of less than 76 cm. At least one muon track must have had an angle of less than 250 mrad with respect to the beam axis. The straight line extrapolation of this track from the target must have passed through the first toroid magnet, and intersected the trigger counter located there. In order to reduce the cosmic ray background for single muon events, accepted events also had to contain at least 2 GeV of hadron energy. No dimuon events failed this cut.

Like Sign Dimuons

The like sign dimuon sample contains 18 ν-induced $\mu^-\mu^-$ events and 1 $\bar{\nu}$-induced $\mu^+\mu^+$ in which each muon traversed at least one toroidal magnet and had a momentum greater than 9 GeV/c. Both muons were required to pass all the appropriate single muon event cuts and to have production angles less than 250 mrad with respect to the beam axis. In addition, both muons must have had fitted tracks which originated in a common vertex consistent with the vertex position along the beam axis obtained from counter pulse height. Each muon's track must have been visible in the spark chambers after the first toroid. Only one of the muon tracks must have an extrapolation to the muon trigger counter.

The single muon sample which was used to normalize the like sign dimuon sample consisted of single muon events that passed the single muon cuts mentioned above and had a magnetically determined muon momentum of $P_\mu > 9$ GeV/c. A total of 117,039 charged current events passed these cuts. The mean total energy and hadron energy of the final like sign dimuon and the normalizing single muon sample passing all cuts are shown in Table 1. Other kinematic quantities are detailed in Table 2.

The principal background sources of like sign dimuons are muon decays of primary π's or K's at the hadron vertex in a charged current event (first generation) and the production of prompt or non-prompt muons from the secondary interactions of the primary hadrons (subsequent generations). To simulate the first generation background, the inclusive primary hadron spectra and multiplicities are obtained from

Table 1. Number, mean measured total energy and mean hadronic energy of single-muon and dimuon events passing all cuts of the like-sign dimuon analysis. The events are binned according to the neutrino energy calculated from the event radius. The errors in the means are shown only if they are greater than 0.5 GeV. The hadron energy cut is $E_H \geqq 2$ GeV

Energy (GeV)	Events	μ^-		Events	$\mu^-\mu^-$	
		E_ν (GeV)	E_H (GeV)		E_ν (GeV)	E_H (GeV)
30–100	66,090	64	25	2	82±18	51±22
100–200	37,927	159	65	11	147±12	68±11
200–230	13,022	215	92	5	189± 5	112±17
30–230	117,039	112	45	18	151±10	78±10

Table 2. Mean kinematic quantities for neutrino-induced single-muon and dimuon events used in the like-sign dimuon analysis, where $Q^2 = 2E_\nu E_{\mu 1}(1-\cos\theta_{\mu 1})$, $\nu = E_\nu - E_{\mu 1}$, $W^2 = M^2 - 2M\nu - Q^2$, $X_{Bj} = Q^2/2M\nu$, and $y = \nu/E_\nu$

Quantity	μ^-	$\mu^-\mu^-$
$p_{\mu 1}$(GeV/c)	66.6 ±0.2	56.3 ± 8.7
Q^2(GeV^2/c^2)	16.4 ±0.1	39.0 ± 7.6
W^2(GeV^2/c^2)	68.9 ±0.2	133.2 ±14.6
x_{Bj}	0.215±0.001	0.21 ± 0.03
y	0.394±0.001	0.51 ± 0.04
$\theta_{\mu 1}$(rad)	0.052±0.001	0.087± 0.014

the Lund Monte Carlo program [3] and checked against BEBC ν-Ne [4] and EMC μ-p data [5]. The contribution of subsequent generations of these hadrons is calculated using the measured prompt and non-prompt muon production by hadrons from Fermilab experiment E379, which used a variable density target [6]. This calculation yields the probability for producing a muon with a momentum greater than a particular cutoff value as a function of the parameters at the quark vertex, particularly the hadron energy, E_H.

The model of the background uses the generated hadron system parameters of Monte Carlo charged current events along with the previously mentioned probabilities to produce background dimuon events with a particular statistical weight and second muon momentum, $P_{\mu 2}$. The generated (second) muon is given a transverse momentum, P_T, with respect to the hadron shower direction based on transverse momentum fits to hadrons from EMC μ-p data [7]. The Monte Carlo events are reconstructed and required to pass the dimuon analysis cuts used for the data. The number of background events is normalized to the number of charged current data events passing the appropriate single muon cuts. We have estimated the systematic error in this procedure to be ±20%. Details of the calculation are presented in Appendix A and [8]. The hadron background for the 18 ν events is calculated to be 10.7±2.1 events. The hadron background for the single $\bar{\nu}$ event is 0.6±0.1 events and we limit subsequent discussion to the ν sample only.

An additional background due to improperly classified trimuon events (originating primarily from hadronic and electromagnetic muon pair production) for which the third muon is hidden in the hadronic shower is estimated to be 0.6±0.2 events. The background from spatially and temporally coincident charged current neutrino events is calculated to be 0.1±0.1 events. The total background of 11.4±2.2 events yields an observed like sign dimuon excess above background of 6.6±4.2±2.2 events, where the first error is statistical and the second error is due to the uncertainty in the level of the background.

If we interpret the small excess of events as a prompt signal and calculate the prompt like sign rate, we need a correction for the limited geometrical acceptance of the apparatus. This acceptance must rely

Table 3. Calculation of the rate of $\mu^-\mu^-/\mu^-$ for the events in Table 2. The μ^- events are corrected for acceptance. From left to right are shown: (1) number of charged current events (acceptance corrected), (2) number of raw $\mu^-\mu^-$ events, (3) the background from the hadron shower, (4) the background from misclassified trimuons and coincident single-muon events, (5) the raw prompt like-sign dimuon signal (after subtraction of all the background). The next three columns show the prompt $\mu^-\mu^-/\mu^-$ rate corrected for acceptance using: (6) a model of π/K decay and shower, (7) $c\bar{c}$ gluon bremsstrahlung model, and (8) $D^0-\bar{D}^0$ mixing. The error includes the 20% systematic error in the hadron shower background

Energy (GeV)	μ^- Evts	$\mu^-\mu^-$ Evts	Hadr Shwr Bkgd	Misc Bkgd	Dat-Bkgd	Prompt $\mu^-\mu^-/\mu^-$ corrected for acceptance with model: ($\times 10^{-4}$)		
						π/K	$c-\bar{c}$	$D^0-\bar{D}^0$
	(1)	(2)	(3)	(4)	(5)	(6)	(7)	(8)
30–100	108,128	2	2.0	0.2	−0.2	−0.1±0.5	−0.1±0.6	−0.1±0.4
100–200	52,930	11	5.7	0.4	4.9	2.4±1.7	2.6±1.8	1.8±1.3
200–300	16,058	5	3.0	0.1	1.9	2.3±2.8	2.3±2.8	1.8±2.2
30–230	177,116	18	10.7	0.7	6.6	1.0±0.7	1.0±0.7	0.8±0.5

Table 4. Comparison of prompt like-sign dimuon rates for several experiments. The beam nomenclature is: NBB for narrow band beam, WBB for wide band horn focussed beam, QTB for quadrupole triplet beam. Note that a WBB has a lower mean neutrino energy

Experiment	Beam Type	p_μ cut (GeV/c)	$\mu^-\mu^-/\mu^-$ prompt $\times 10^{-4}$	$\mu^-\mu^-/\mu^-\mu^+$ prompt $\times 10^{-2}$	Ref.
CCFRR	NBB	9	1.0 ± 0.7	4.0 ± 2.9	this exp.
CDHS	WBB	6.5	0.43 ± 0.23	4.2 ± 2.3	[11]
CDHS	NBB, WBB	9	1.16 ± 0.42	3.2 ± 1.2	[12]
CHARM	WBB	4	4.5 ± 1.6	14 ± 5	[13]
HPWFOR	QTB	10	3.0 ± 0.8	7 ± 4	[14]
CFNRR	QTB	9	2.0 ± 1.1	–	[15]

on a specific model. In the absence of such a model, we have assumed the distribution of prompt dimuon events to be the same as that of the non-prompt background. The acceptance corrected ratio of like sign dimuon production to single muon production thereby obtained is $(1.0 \pm 0.7) \times 10^{-4}$. The acceptance has also been calculated using a model of the gluon bremsstrahlung of charm-anticharm quark pairs with the anticharm quark decay producing the second muon [9]. Although the contribution to like sign dimuons from $D^0 - \bar{D}^0$ mixing is expected to be negligible [10], we have also calculated the acceptance using this model for completeness. The rates calculated with the π and K decay model acceptance are presented in Table 3 with a comparison of rates using the acceptance correction for $c\bar{c}$ production and $D^0 - \bar{D}^0$ mixing. The acceptance does not depend substantially on whether the π and K decay or $c\bar{c}$ models are used and is somewhat higher for the $D^0 - \bar{D}^0$ model.

A comparison of our results with the prompt like sign and opposite sign rates from other experiments is shown in Table 4. The energy dependence of the prompt like sign dimuon to charged current rate is shown in Fig. 2. The curve in Fig. 2 is the prompt signal calculated from the charm-anticharm production model of [9], assuming $\alpha_s = 0.2$ and $m_c = 1.5$ GeV/c^2. This calculated signal scales with α_s^2 and yields 0.2 events for this experiment.

In addition to the overall rates, the distributions of kinematic quantities for the observed like sign events can be compared with those expected from the π and K decay background. Distributions of several kinematic variables for the like sign dimuons and Monte Carlo events from π and K decay are compared in Fig.3, and the means of these distributions are summarized in Table 5. The π and K decay histograms, shown as dashed lines, are normalized to 10.7 events. The distribution of the angle between the two muon tracks projected on a plane perpendicular to the incident neutrino is shown in Fig. 3a. The peaking

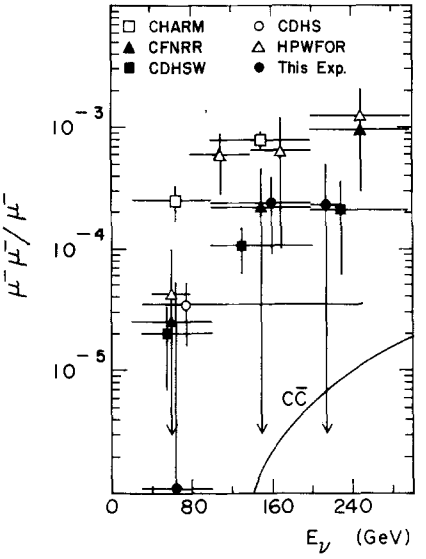

Fig. 2. Like sign dimuon rates. The rates for prompt $\nu N \to \mu^-\mu^- x$ relative to the single muon charged current cross section are presented. The data include the momentum cut for the second muon listed in Table 4. The $c\bar{c}$ gluon bremsstrahlung model used is that of [14] with a momentum cut of 9 GeV/c on the produced muon

of this distribution near 180° indicates that the second muon is associated with the hadron vertex as is expected for π and K decay.

We define the second muon to be that which has the smaller momentum in the direction perpendicular to the axis of the hadron shower ($P_{\perp 2\,\min}$). The hadron shower direction is determined from the incoming ν beam properties and the measured vector momentum of the chosen first muon. Figure 3b shows the $(P_{\perp 2\,\min})^2$ distribution. There is a single event with a $(P_{\perp 2\,\min})^2$ of 6.0 (GeV/c)^2, which is unlikely to be from π and K decay. Such an event could originate from the trimuon and overlap backgrounds, which were estimated to total 0.7 events. Figure 3c displays the momentum of the second muon as defined above.

Figure 3d shows the distribution of missing energy for all like sign ν_K dimuon events. The missing

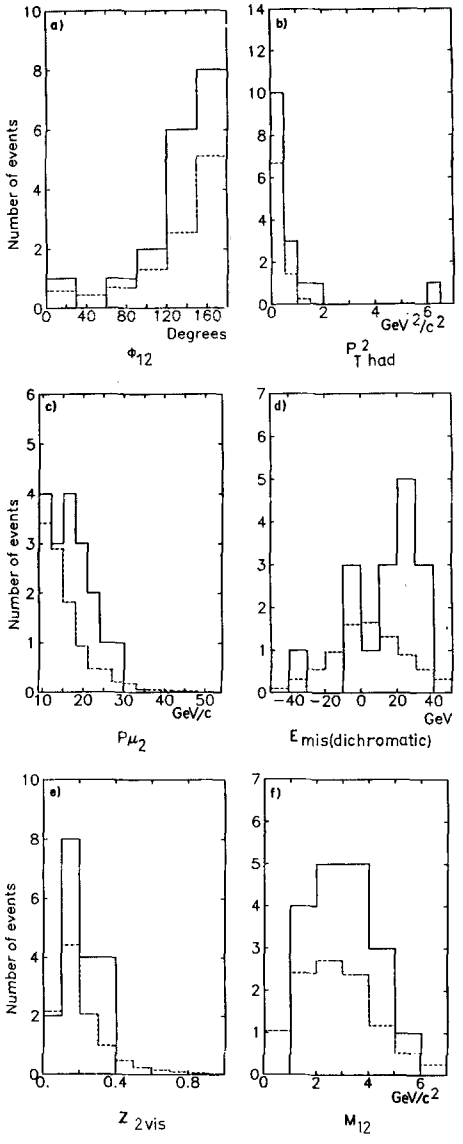

Fig. 3a–f. Distributions of kinematic quantities from like sign dimuon data (solid line) and the π/K decay background (dashed line). **a** shows the angle between the two muons in the plane perpendicular to the incident neutrino direction; **b** shows the square of the transverse momentum of the chosen second muon with respect to the hadron shower direction; **c** shows the momentum of the chosen second muon; **d** shows the missing energy of the ν_K line sign dimuon events; **e** shows the observed fragmentation $Z_{\mu_2}=P_{\mu_2}/(E_H+P_{\mu_2})$; **f** shows the invariant mass of the muon pair

energy is the difference between the neutrino energy determined by the transverse vertex radius and the measured energy. These two measurements agree for single muon events. The missing energy for the data is 2.2 standard deviations greater than that expected for π and K decay. The distribution of $Z_{\mu_2}=P_{\mu_2}/(E_H+P_{\mu_2})$ is shown in Fig. 3e and the distribution of the invariant mass of the $\mu^-\mu^-$ pair is shown in Fig. 3f. There is no evidence of any structure in the mass distribution of the data. In conclusion, the shapes of

Table 5. Means of kinematic distributions of like-sign dimuon data, the π/K decay background, and a combination of π/K decay and $c\bar{c}$ gluon bremsstrahlung models. The $c\bar{c}$ number of events is multiplied by a factor 42 to equal the prompt like-sign dimuon signal. The errors on the means are shown in parentheses. The missing energy is calculated for the 16 identified ν_K ($E_\nu > 100$ GeV) events only, and its error includes an overall 1.2 GeV systematic error. The transverse momentum of the second muon with respect to the hadron shower is also calculated only for ν_K events. A similar comparison for opposite-sign dimuon events is shown in Table 8

Quantity	Data (raw)	Hadron Sh. Background	Hadron Sh. + $c-\bar{c}\times 42$
ϕ_{12}(degrees)	139 (9)	133 (1)	129 (1)
$p^2_{T2\,min}$(GeV^2/c^2)	0.80 (0.35)	0.37 (0.02)	0.46 (0.03)
$p_{\mu 2}$(GeV/c)	17.1 (1.3)	16.4 (0.3)	18.2 (0.2)
E_{mis}(GeV)	17.5 (4.5)	7.2 (1.5)	8.1 (1.6)
$z_{\mu 2}$	0.21 (0.02)	0.21 (0.01)	0.19 (0.01)
M_{12}(GeV/c^2)	3.1 (0.3)	2.8 (0.1)	2.9 (0.1)

the kinematic distributions are similar to those from the π and K decay background with the possible exception of the missing energy and P_T distributions.

It has been suggested [16] that enhanced $c\bar{c}$ production could account for the prompt like sign dimuon signal. In Fig. 4 kinematic distributions of the data are compared with the distributions of the sum of the expected 11.4 background events and the predicted distribution of $c\bar{c}$ Monte Carlo events normalized (by a factor of 42) to the 6.6 remaining events. The means of the distributions are compared in Table 5. The kinematics from the $c\bar{c}$ model do not sufficiently differ from those of π and K decay to allow the source of prompt events to be identified. The mean missing energy predicted for this combination of $c\bar{c}$ and π/K decay models is 2.0 standard deviations removed from that of the data.

The observed like sign dimuon signal of 6.6 ± 4.8 events is 1.4 standard deviations above the background. Most distributions of the data are similar to those expected from π/K decay or $c\bar{c}$ production. The missing energy and P_T kinematic distributions of the data differ somewhat from predictions obtained with these two models. Nevertheless, these data are consistent with the absence of same sign dimuon production. Averaged over the energy range, $30<E_\nu<230$ GeV, we place a 90% confidence level upper limit on the prompt $\mu^-\mu^-/\mu^-$ rate for $P_\mu>9$ GeV/c of 2.3×10^{-4}.

Opposite Sign Dimuons

The opposite sign dimuon event selection criteria are similar to those for the like sign dimuons, but differ in detail. The ν_K events are required to have a transverse vertex within a 1.3 m radius of the neutrino

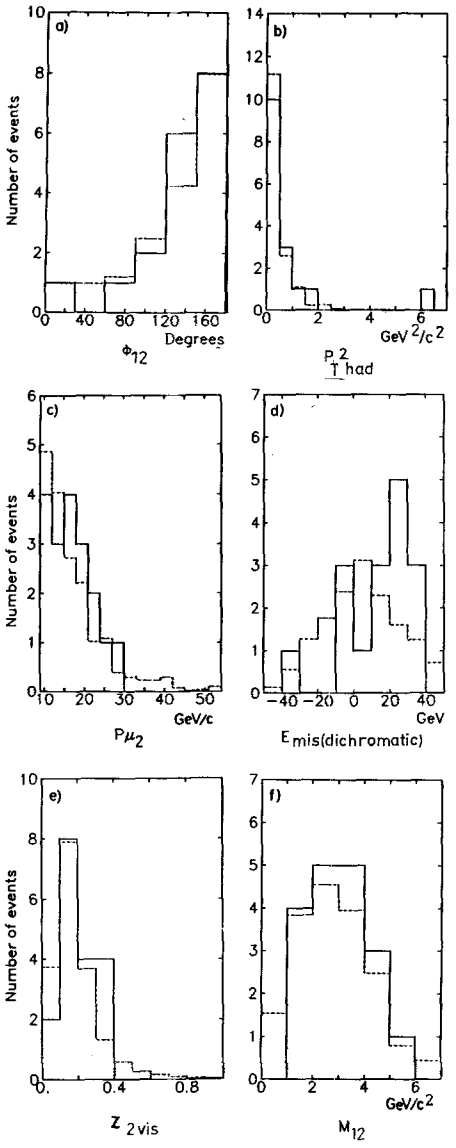

Fig. 4a–f. Distributions of the kinematic quantities displayed in Fig. 3 for like sign dimuon data (solid line) and the π/K decay background with 42 times the $c\bar{c}$ gluon bremsstrahlung model added (dashed line)

beam center. The angle cut on the second muon is 350 mrad. In addition, the muon momentum must be greater than 4.3 GeV/c for both muons. Although for $P_\mu < 9$ GeV/c, the efficiency for full momentum reconstruction in the toroids of a muon is small, a lower limit on the momentum can be determined from the energy loss calculated from the observed distance traversed in steel. The 4.3 GeV/c cut is imposed by requiring that the muon pass through a distance of 3.1 m in steel. Therefore the opposite sign dimuon analysis requires a longitudinal vertex coordinate at least 5.9 m from the downstream end of the target. This restricts the target fiducial volume. The analysis also requires a first muon angle of less than 150 mrad with respect to the beam axis.

Table 6a. Number, mean measured total energy and mean hadronic energy of neutrino induced single-muon and dimuon events passing all cuts of the opposite-sign dimuon analysis, $p_\mu > 4.3$ GeV/c. The events are binned according to the neutrino energy calculated from the event radius. The errors in the means are shown only if they are greater than 0.5 GeV. The hadron energy cut is $E_H \geqq 2$ GeV

Energy (GeV)	Events	μ^-		Events	$\mu^-\mu^+$	
		E_ν (GeV)	E_H (GeV)		E_ν (GeV)	E_H (GeV)
30–100	52,258	64	24	135	66±2	26±2
100–180	19,727	149	60	131	141±2	63±3
180–230	18,761	203	85	171	187±2	81±3
30–230	90,746	111	45	437	136±3	59±2

Table 6b. Number, mean measured total energy and mean hadronic energy of antineutrino induced single-muon and dimuon events passing all cuts of the opposite-sign dimuon analysis. The events are binned according to the neutrino energy calculated from the event radius. The errors in the means are shown only if they are greater than 0.5 GeV. The hadron energy cut is $E_H \geqq 2$ GeV

Energy (GeV)	Events	μ^+		Events	$\mu^+\mu^-$	
		E_ν (GeV)	E_H (GeV)		E_ν (GeV)	E_H (GeV)
30–100	8,646	61	19	16	62±4	24±3
100–230	2,277	155	50	15	141±7	48±6
30–230	10,923	80	25	31	100±8	36±4

The number and mean energy of the single muon and dimuon events used in the opposite sign analysis is shown in Table 6. The single muon sample used to normalize the opposite sign dimuon analysis is different from that used in the like sign dimuon analysis due to the reduced fiducial volume and consists of 90,746 ν and 10,923 $\bar{\nu}$ charged current events. After the cuts defined above are applied, there are 437 opposite sign dimuons produced by neutrinos and 31 from antineutrinos. The characteristics of the opposite sign dimuons and single muons are detailed in Table 7. The calculated π and K decay background is 106±21 for the neutrino sample and 7±1 for the antineutrino sample. The background includes events with muons of both signs for which a lower limit on the second muon momentum is determined by range in the target only.

Experiments in bubble chambers [17] and emulsions [18] have directly observed single charm production and decay which are consistent with being the dominant source of the prompt opposite sign dimuon signal in neutrino interactions. Within the framework of the standard quark model, the rate for production of charmed quarks by neutrinos is proportional to $d(x)\sin^2\theta_c + s(x)\cos^2\theta_c$, where θ_c is the

Table 7. Mean measured kinematic quantities for single-muon and dimuon events with $p_\mu > 4.3$ GeV/c used in the opposite-sign dimuon analysis (no background subtracted). Statistical errors are shown in parentheses

Quantity	ν		$\bar{\nu}$	
	μ^-	$\mu^-\mu^+$	μ^+	$\mu^+\mu^-$
p_μ(GeV/c)	66.7	66.4	55.4	56.2
	(0.2)	(2.1)	(0.5)	(5.2)
Q^2(GeV^2/c^2)	15.3	19.5	7.7	10.8
	(0.1)	(1.0)	(0.1)	(2.4)
W^2(GeV^2/c^4)	68.9	111.9	40.7	73.0
	(0.3)	(3.6)	(0.5)	(8.3)
x_{Bj}	0.208	0.17	0.202	0.14
	(0.001)	(0.01)	(0.002)	(0.03)
y	0.392	0.42	0.313	0.35
	(0.001)	(0.01)	(0.002)	(0.02)
θ_μ(rad)	0.050	0.052	0.044	0.046
	(0.001)	(0.002)	(0.001)	(0.005)

Cabibbo angle and $d(x)$ and $s(x)$ are the quark density distributions in the proton as functions of the fractional momentum $x = Q^2/2\,m\nu$, where $Q^2 = 2\,E_\nu E_\mu(1-\cos\theta_\mu)$ and $\nu = E_\nu - E_\mu$. The rate of production of anticharm by antineutrinos is proportional to $\bar{d}(x)\sin^2\theta_c + \bar{s}(x)\cos^2\theta_c$. The neutrino rate has contributions from both valence down quarks and sea strange quarks, while the antineutrino rate is primarily due to the antistrange sea.

The $V-A$ structure of the weak interaction implies that neutrino and antineutrino production of charm (in the absence of scaling violation and threshold effects) is uniform in y because the production is from quarks for neutrinos and antiquarks for antineutrinos. However, the threshold for production of charm shifts the y distribution toward higher y. To create a charmed quark with mass, m_c, the fraction of nucleon momentum carried by the light quark, $x = Q^2/2\,M\nu$, is actually $x' = x + (m_c^2/2\,M\nu)$. In the calculation of charm production [19], x' is substituted for x as the appropriate scaling variable (slow rescaling) and a phase space factor for producing a heavy quark in two body scattering is included. The differential cross section for charmed hadron production is then [20]:

$$\frac{d^3\sigma}{dx'\,dy\,dZ} = \frac{G^2 M E_\nu}{\pi}\left[x'd(x')\sin^2\theta_c + x's(x')\cos^2\theta_c\right] \cdot\left[1-\frac{m_c^2}{2ME_\nu x'}\right]D(Z).$$

The fragmentation function of the charmed quark is $D(Z)$ where Z is the fraction of the available energy taken by the charmed particle (e.g. D meson) in the W boson-nucleon center of mass frame.

Neutrino production of charm was simulated with a Monte Carlo calculation that used both valence quark and sea quark x distributions extracted from CCFRR data [21]. These distributions are shown in Fig. 5. As expected, the kinematic distributions of the single muon data and those of the Monte Carlo events agree well. Figure 6 shows the x and y distributions for single muon data and Monte Carlo events used in the single muon $\mu^+\mu^-$ normalization sample.

The model of neutrino production of charm requires input information about the charmed quark mass (m_c), charmed meson transverse momentum relative to the outgoing quark direction, (P_T), semileptonic branching ratio (B), and fragmentation (D). The charmed quark mass is assumed to be $m_c = 1.5$ GeV/c^2, unless otherwise stated. The transverse

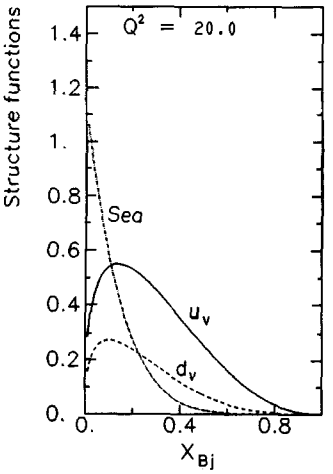

Fig. 5. Valence and sea x distributions extracted from CCFRR data [21] at a mean Q^2 of 20 GeV^2/c^2

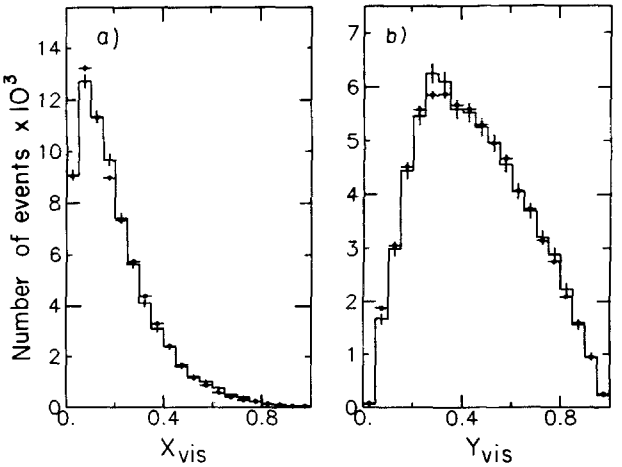

Fig. 6a, b. Distribution of **a** Bjorken x, and **b** the scaling variable y for single muon charged current events with $E_H > 10$GeV. The points with error bars represent the data and the histogram represents the Monte Carlo events

momentum distribution of the charmed mesons with respect to the hadron shower direction is taken to be $e^{-1.1 P_T^2}$ according to LEBC/EHS hadronic charm production data [22]. The charm branching ratio to muons, $B=(10.9\pm1.4)\%$, is determined from the branching ratio of the mixture of charmed particles found in e^+e^- reactions [23] when applied to the composition of charm particles found in the neutrino emulsion data [18]. Details of the branching ratio calculation and modeling of the charmed semileptonic decay are contained in Appendix B. The data presented here are consistent with this branching ratio and use this value of B as an input constraint. It should be pointed out that previous dimuon analyses [24] obtained values for B that were lower. Lower values had also been suggested by previous e^+e^- measurements [25].

The fragmentation of charm has been studied in e^+e^- interactions. The mean invariant mass of the final state hadron system, $W=\sqrt{M^2+2Mv-Q^2}$, of our single muon events is 8 GeV/c^2 and therefore we use the measurements of the Argus collaboration [26] taken at a c.m. energy of 10 GeV which approximately corresponds to the W of neutrino interactions. The Argus group fits the charm fragmentation of D^{*+} mesons with the form of Peterson et al. [27]:

$$D(Z)\propto\frac{1}{Z\left(1-\frac{1}{Z}-\frac{\varepsilon}{(1-Z)}\right)^2}$$

where $Z=P_D/P_{\max}$ and $P_{\max}=\sqrt{E_{\text{beam}}^2-M_{D^*}^2}$. The Argus group reported $\varepsilon=0.19\pm0.03$. Our model of charm fragmentation uses the definition of Z in neutrino reactions where $E_{\text{beam}}=W/2$. For this definition, the fragmentation takes place in the W boson-nucleon center of mass. To cover the wide range in values of ε reported by various other experiments [28], we have studied the sensitivity of our results to the value of ε using $\varepsilon=0.09$, 0.19 and 0.29.

Kinematic distributions of the background subtracted opposite sign dimuon data and the charm Monte Carlo (with $m_c=1.5$ GeV/c^2 and $\varepsilon=0.19$) are shown in Fig. 7. The means of these distributions are given in Table 8. The distributions shown in Fig. 7 are similar to those presented in Figs. 3 and 4 for the like sign dimuons. For purposes of this comparison, the opposite sign dimuons are required to have momentum analyzed muons with $P_\mu>9$ GeV/c and to pass all of the like sign dimuon analysis cuts. The number of opposite sign dimuon events passing these cuts is 199. The π and K decay background is 12 ± 2 events, leaving a prompt signal of 187 ± 14 events. The agreement between the model and data is good for all distributions, including missing energy. The

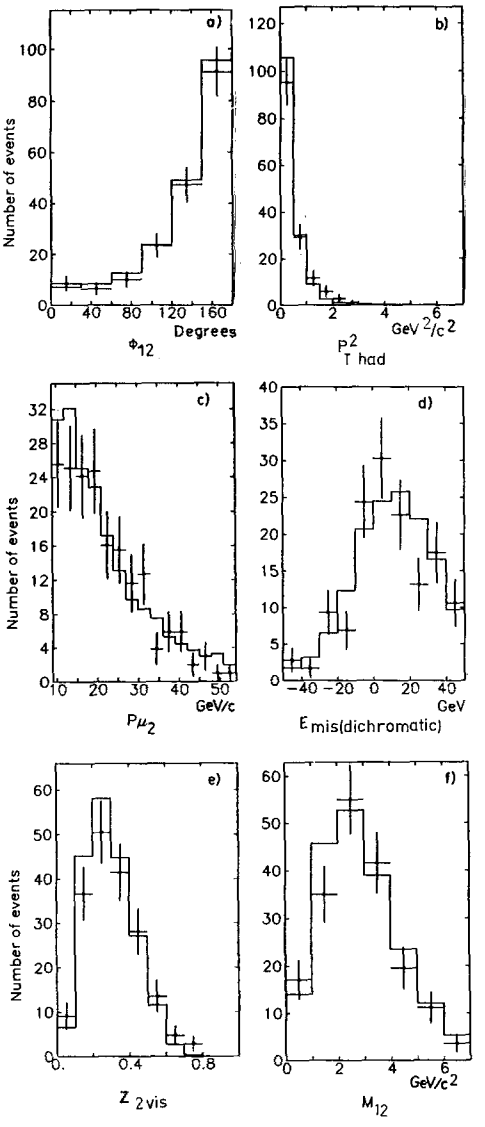

Fig. 7a–f. Distributions of the kinematic quantities displayed in Fig. 3 for opposite sign dimuon events with the π/K decay background subtracted (points with error bars) and the single charm opposite sign dimuon model (solid line)

acceptance corrected prompt rate $\mu^-\mu^-/\mu^+\mu^-$ for $P_\mu>9$ GeV/c is $4.0\pm2.9\%$.

The charm Monte Carlo is used to correct the background subtracted opposite sign dimuon data for acceptance. Figure 8a shows the observed ratio $\sigma(2\,\mu)/\sigma(1\,\mu)$ vs. energy for $P_\mu>4.3$ GeV/c. The calculated background versus neutrino energy is shown on the same figure as the lower points. The raw 2 μ background/1 μ rate increases linearly with energy and reaches $(2.3\pm0.5)\times10^{-3}$ at $E_\nu=200$ GeV. Figure 8b shows the measured 2 μ/1 μ rate after subtraction of the background. Figure 8c shows the 2 μ/1 μ rate, this time also corrected for geometric acceptance. Figure 8d shows the 2 μ/1 μ rate after correction for the

Table 8. Means of kinematic distributions of opposite-sign dimuons with hadron shower background subtracted along with means of distributions obtained from the charm Monte Carlo. All events have the momentum of both muons magnetically analyzed with $p_\mu > 9$ GeV/c. The errors on the means are shown in parentheses. The missing energy is calculated for the 158 identified ν_K ($E_\nu > 100$ GeV) events only, and its error includes an overall 1.2 GeV systematic error. The transverse momentum of the positive muon with respect to the hadron shower direction is also calculated for ν_k events

Quantity	Data with backgr. subtracted	Charm production Monte Carlo
ϕ_{12}(degrees)	136 (3)	135 (1)
$p^2_{T2\,min}$(GeV^2/c^2)	0.50 (0.05)	0.47 (0.01)
$p_{\mu 2}$(GeV/c)	24.4 (0.4)	23.5 (0.2)
E_{mis}(GeV)	14.5 (2.2)	15.4 (0.7)
$z_{\mu 2}$	0.31 (0.01)	0.30 (0.01)
M_{12}(GeV/c^2)	2.9 (0.1)	3.0 (0.1)

$P_\mu > 4.3$ GeV/c cut using the charm Monte Carlo. These rates are thus fully corrected for geometric and muon momentum acceptance, and for the π and K decay background. The fully corrected prompt 2 μ/1 μ rate rises to $(9.0 \pm 1.1) \times 10^{-3}$ at $E_\nu = 200$ GeV. Figure 9 shows the corresponding 2 μ/1 μ rates for antineutrinos. The raw background 2 μ/1 μ rate is $(1.3 \pm 0.3) \times 10^{-3}$ at $E_{\bar\nu} = 160$ GeV. The fully corrected prompt 2 μ/1 μ rate at this energy is $(8.4 \pm 2.7) \times 10^{-3}$. Tables 9 and 10 contain the results illustrated in Figs. 8 and 9.

The threshold for charm production is modeled by the slow rescaling substitution of x' for x, as noted previously [20]. Using the charm Monte Carlo and the slow rescaling procedure, we have investigated the effects of the finite charm quark mass. In principle, the slow rescaling correction should remove the energy dependence of the prompt dimuon rates except for a small Q^2 dependence of the strange sea. The energy dependence of the $\sigma(2\,\mu)/\sigma(1\,\mu)$ rate after correction for slow rescaling (with m_c assumed to be 1.0, 1.5, and 1.9) is shown in Fig. 10a (for neutrinos) and Fig. 10b (for antineutrinos). A summary of the energy dependence of the $\sigma(2\,\mu)/\sigma(1\,\mu)$ rate is presented in Table 10a for neutrinos and Table 10b for antineutrinos. Values of m_c greater than 1.5 GeV/c^2 are suggested. As is discussed below, an energy dependence of the semileptonic branching ratio of charm states would affect this conclusion. A comparison of the energy dependence of the prompt opposite sign dimuon rate found by this experiment and that seen in the CDHS wide band data [24] is shown in Fig. 11 for

Table 9a. Raw and corrected numbers of neutrino induced opposite sign dimuon and single-muon events with $p_\mu > 4.3$ GeV/c. From left to right are shown: (1) the number of charged-current events corrected for geometric acceptance, (2) the number of charged-current events corrected for momentum acceptance ($p_\mu > 0$), (3) the number of raw opposite-sign dimuon events, (4) the number of raw dimuon background events from hadron shower, (5) the raw opposite-sign dimuon data with the hadron background subtracted, (6) the background subtracted dimuon data corrected for geometric acceptance, (7) the background subtracted dimuon data corrected for geometric and momentum acceptance ($p_\mu > 0$), (8) the background subtracted dimuon data corrected for acceptance and the charm quark mass threshold (slow rescaling correction) with the charm quark mass $m_c = 1.0$ GeV/c^2, (9) as in (8) with $m_c = 1.5$ GeV/c^2, (10) as in (8) with $m_c = 1.9$ GeV/c^2. The errors shown in parentheses include statistics and the 20% uncertainty in the background subtraction

Energy (GeV)	(1)	(2)	(3)	(4)	(5)	(6)	(7)	(8)	(9)	(10)
30–100	63294 (277)	85996 (376)	135 (12)	34 (7)	101 (14)	201 (27)	409 (55)	582 (78)	698 (94)	822 (110)
100–180	23921 (170)	2818 (201)	131 (11)	28 (6)	103 (13)	166 (21)	228 (28)	265 (33)	292 (36)	321 (40)
180–230	21705 (158)	23797 (174)	171 (13)	44 (9)	127 (16)	168 (21)	215 (27)	246 (30)	263 (33)	284 (35)
30–230	108920 (362)	137974 (458)	437 (21)	106 (21)	331 (30)	535 (48)	852 (77)	1093 (98)	1253 (113)	1427 (128)

Table 9b. Raw and corrected numbers of antineutrino induced opposite-sign dimuon and single-muon events as in **9a**

Energy Bin (GeV)	(1)	(2)	(3)	(4)	(5)	(6)	(7)	(8)	(9)	(10)
30–100	9800 (105)	11912 (128)	16 (4)	4 (1)	12 (4)	22 (7)	45 (15)	66 (22)	87 (30)	109 (37)
100–230	2497 (52)	2729 (57)	15 (4)	3 (1)	12 (4)	17 (6)	23 (7)	28 (9)	32 (10)	36 (12)
30–230	12297 (118)	14641 (140)	31 (6)	7 (1)	24 (6)	39 (9)	68 (16)	94 (22)	119 (28)	145 (35)

Table 10a. Ratio of neutrino induced opposite-sign dimuon events to single-muon events. Shown are: (1) raw observed rates, $\pi_\mu > 4.3$ GeV/c, (2) the hadron shower background rate, (3) the background subtracted raw dimuon rates, $p_\mu > 4.3$ GeV/c, (4) the background subtracted dimuon rates corrected for geometric acceptance, $p_\mu > 4.3$ GeV/c, (5) the background subtracted dimuon rates corrected for geometric and momentum acceptance $p_\mu > 0$, (6) the background subtracted acceptance corrected rates further corrected for the charm quark mass threshold (slow rescaling), $m_c = 1.0$ GeV/c^2, (7) as in (6) with $m_c = 1.5$ GeV/c^2, (8) as in (6) with $m_c = 1.9$ GeV/c^2. Errors shown in parentheses include statistics and 20% uncertainty in the background. Entries are in units of 10^{-3}

Energy (GeV)	(1)	(2)	(3)	(4)	(5)	(6)	(7)	(8)
30–100	2.6	0.7	1.9	3.2	4.8	6.8	8.1	9.6
	(0.2)	(0.1)	(0.3)	(0.4)	(0.6)	(0.9)	(1.1)	(1.3)
100–180	6.6	1.4	5.2	6.9	8.1	9.4	10.4	11.9
	(0.6)	(0.3)	(0.7)	(0.9)	(1.0)	(1.2)	(1.3)	(1.4)
180–230	9.1	2.3	6.8	7.7	9.0	10.4	11.4	11.9
	(0.6)	(0.3)	(0.7)	(0.9)	(1.0)	(1.2)	(1.3)	(1.4)
30–230	4.8	1.1	3.7	4.9	6.2	7.9	9.1	10.3
	(0.2)	(0.2)	(0.3)	(0.4)	(0.6)	(0.7)	(0.8)	(0.9)

Table 10b. Ratio of antineutrino induced opposite-sign dimuon events to single-muon events as in **10a**

Energy (GeV)	(1)	(2)	(3)	(4)	(5)	(6)	(7)	(8)
30–100	1.9	0.5	1.4	2.2	3.8	5.5	7.3	9.2
	(0.5)	(0.1)	(0.5)	(0.8)	(1.3)	(1.9)	(2.5)	(3.1)
100–230	6.6	1.3	5.3	6.8	8.5	10.3	11.6	13.1
	(1.7)	(0.3)	(1.7)	(2.2)	(2.7)	(3.3)	(3.8)	(4.2)
30–230	2.8	0.6	2.2	3.2	4.6	6.4	8.1	9.9
	(0.5)	(0.1)	(0.5)	(0.8)	(1.1)	(1.5)	(1.9)	(2.4)

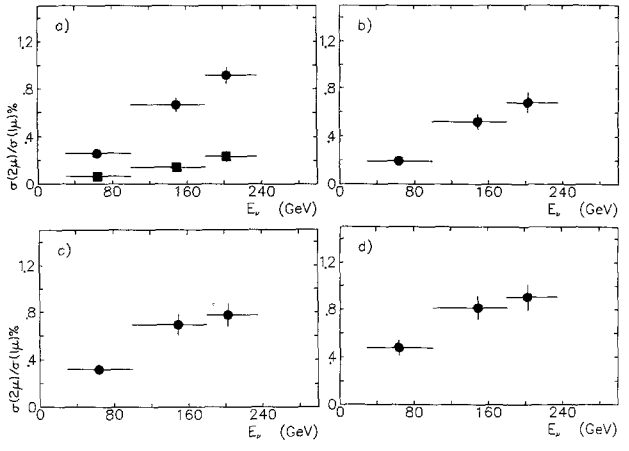

Fig. 8a–d. Energy dependence of neutrino induced opposite sign dimuon rates: **a** raw data (circles) and raw background (squares) ($p_\mu > 4.3$ GeV/c); **b** raw data with the background subtracted ($p_\mu > 4.3$ GeV/c); **c** data with the background subtracted corrected for geometrical acceptance ($p_\mu > 4.3$ GeV/c); **d** as in **c** with additional correction for muon momentum cut (yielding rates for $p_\mu > 0$ GeV/c)

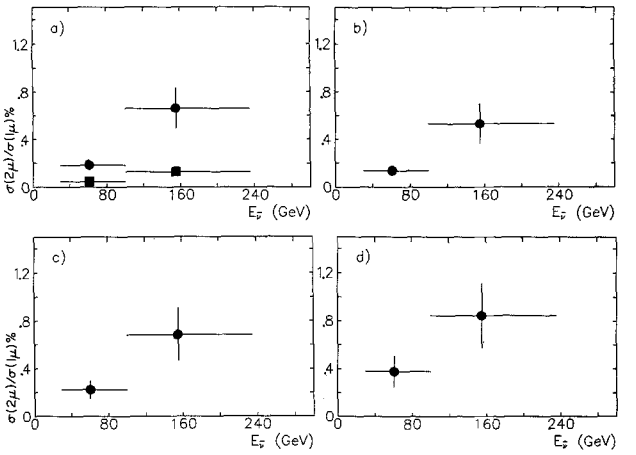

Fig. 9a–d. Energy dependence of antineutrino induced opposite sign dimuon rates. **a** raw data (circles) and raw background (squares) ($p_\mu > 4.3$ GeV/c); **b** raw data with the background subtracted ($p_\mu > 4.3$ GeV/c); **c** data with the background subtracted corrected for geometrical acceptance ($p_\mu > 4.3$ GeV/c); **d** as in **c** with additional correction for muon momentum cut (yielding rates for $p_\mu > 0$ GeV/c)

neutrinos and Fig. 12 for antineutrinos. Figure 11a and 12a show the data fully corrected for geometric acceptance and the muon momentum cut. Figures 11b and 12b show the data corrected for the effect of the charm mass threshold of 1.5 GeV/c^2.

The amount of strange sea in the nucleon can be determined from the magnitude and shape of the x distributions for the prompt neutrino and antineutrino opposite sign dimuons. The number of events is compared to the corresponding number of charm Monte Carlo events by forming a χ^2 for seven x bins for neutrino data and one bin (all x) for the antineu-

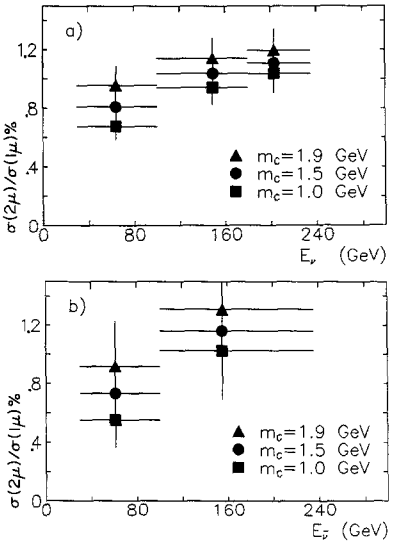

Fig. 10a, b. Energy dependence of **a** neutrino and **b** antineutrino induced opposite sign dimuon rates fully corrected for geometrical acceptance and muon momentum cut, and also corrected for the slow rescaling with three charm quark masses of 1.0, 1.5, and 1.9 GeV/c^2

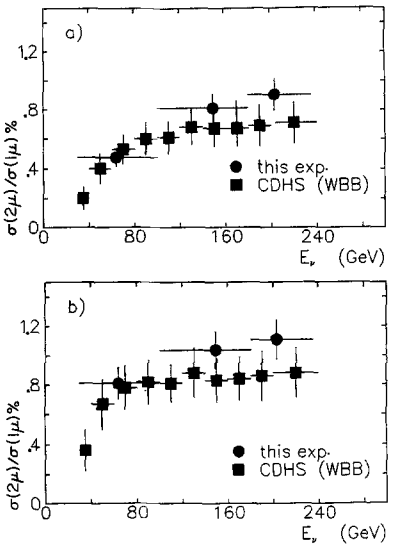

Fig. 11a, b. Comparison of the energy dependence of neutrino induced opposite sign dimuon rates from this experiment and the CDHS experiment at CERN. The squares show CDHS results [14] with the wide band beam. Part **a** presents rates corrected for geometrical acceptance and the muon momentum cut; part **b** shows the rates with an additional correction for slow rescaling with $m_c = 1.5$ GeV/c^2

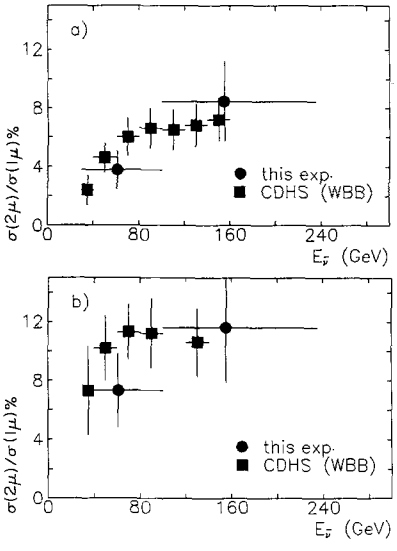

Fig. 12a, b. Comparison of the energy dependence of antineutrino induced opposite sign dimuon rates from this experiment and the CDHS experiment at CERN. The squares show the CDHS results [24] with the wide band beam. Part **a** presents rates corrected for geometrical acceptance and muon momentum cut, part **b** shows the rates with an additional correction for slow rescaling with $m_c = 1.5$ GeV/c^2

trino data. We assume $s(x) = \frac{\kappa}{2}[\bar{u}(x) + \bar{d}(x)]$ and fit for κ. The value of κ is used to extract the amount of strange sea, η_s:

$$\eta_s = \frac{2\int x s(x)\,dx}{\int x[u(x)+d(x)]\,dx} = \frac{\kappa \int x[\bar{u}(x)+\bar{d}(x)]\,dx}{\int x[u(x)+d(x)]\,dx}.$$

The best fit values of κ and the charm branching ratio (B) to muons are highly correlated. Therefore, the χ^2 surface is shown as a function of $\kappa \cdot B$ vs. B in Fig. 13a with the 1, 2 and 3 standard deviation contours. We find the values:

$$\kappa = 0.56^{+0.81}_{-0.18} \quad \text{and} \quad B = 0.086 \pm 0.016.$$

A better fit for κ can be made by imposing the input constraint on B of $10.9 \pm 1.4\%$ described previously. The χ^2 surface as a function of κ alone and B is shown in Fig.13b. The systematic error caused by the $\pm 20\%$ uncertainty in the non-prompt background is calculated by repeating the fits with this background multiplied by 1.2 and 0.8, respectively. The fit resulted in a measurement of $\kappa = 0.42^{+0.13}_{-0.10} \pm 0.02$, where the first error includes the statistical error and the uncertainty in the charm branching ratio, and the second error is due to the uncertainty in the level of the background. The value of κ corresponds to $\eta_s = 0.063^{+0.016}_{-0.013} \pm 0.003$, where the ratios of the nucleon quark content (q) and antiquark content ($\bar{q}$), $\bar{q}/q = 0.175$ and $\bar{q}/(q+\bar{q}) = 0.149$, were used [21]. Figure 14 shows the agreement between x and y distributions of neutrino induced background-subtracted dimuon data with the single charm Monte Carlo calculation for this value of κ.

The extraction of κ using this method is strongly dependent on the charm branching ratio. A direct measurement of the branching ratio that is less dependent on κ can be made by examining $\sigma(2\,\mu)/\sigma(1\,\mu)$

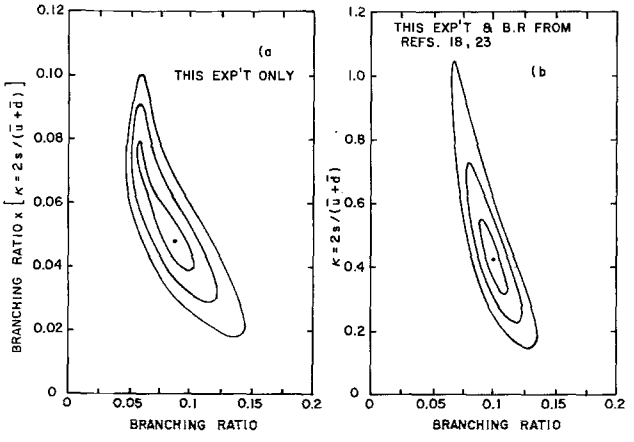

Fig. 13a, b. χ^2 contours as a function of the charm semileptonic branching ratio (B) vs. $\kappa \cdot B$ **a** and κ **b** from fits to ν and $\bar{\nu}$ x-distributions of opposite sign dimuon events. Shown are the 1, 2, and 3 standard deviation contours for $\varepsilon = 0.19$ and $m_c = 1.5$ GeV/c^2. In **b** the results are constrained to be consistent with value of $B = 10.9 \pm 1.4\%$

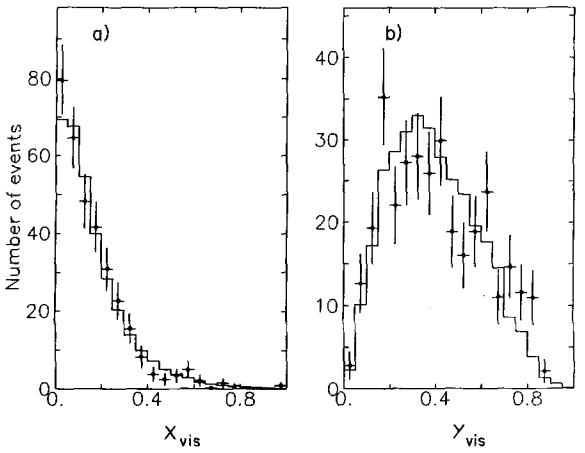

Fig. 14a, b. Distribution of **a** Bjorken x, and **b** the scaling variable y for the opposite sign background subtracted dimuon data with $P_\mu > 4.3$ GeV/c (points with error bars) and the single charm Monte Carlo (solid line)

for $x > 0.25$, where the contribution of valence quarks dominates over that of the sea quarks (see Fig. 5). Assuming $m_c = 1.5$ and $\varepsilon = 0.19$, we find a charm branching ratio to muons of $0.080^{+0.022+0.003+0.050}_{-0.011-0.006-0.005}$, where the first error is the statistical error, the second error is from the systematic errors in the background subtraction ($\pm 20\%$), and the third error is from the variation in κ over the range from 0 to 1. This result is consistent with the value of 0.109 ± 0.014 extracted from the e^+e^- and neutrino emulsion data as mentioned above.

Figure 15 shows the fit values of κ for a wide range of branching ratios. The solid lines are the best fit values for the nominal choice of background and the parameters $m_c = 1.5$, $\varepsilon = 0.19$. Figure 15a shows the best fit values with the π and K decay background subtraction at its nominal value and both increased and decreased by its 20% systematic normalization error. Figure 15b shows the fit for three values of the charm quark mass, $m_c = 1.0$, 1.5 and 1.9 GeV/c^2 with $\varepsilon = 0.19$ in the Peterson et al. fragmentation formula. Figure 15c shows the fit with $m_c = 1.5$ GeV/c^2 and the values of the Peterson et al. fragmentation parameter, $\varepsilon = 0.09$, 0.19 and 0.29. In addition, Fig. 15d shows the fit with the fragmentation formula $D(Z) = \delta(Z - 0.68)$. From these studies we estimate uncertainties in κ of ± 0.08 and ± 0.02 due to changes in the charm quark mass and fragmentation functions, respectively. Combining these errors in quadrature gives $\kappa = 0.42^{+0.15}_{-0.13}$, which is equivalent to $\eta_s = 0.063^{+0.018}_{-0.017}$. The results for different fragmentation and charm quark masses are summarized in Table 11.

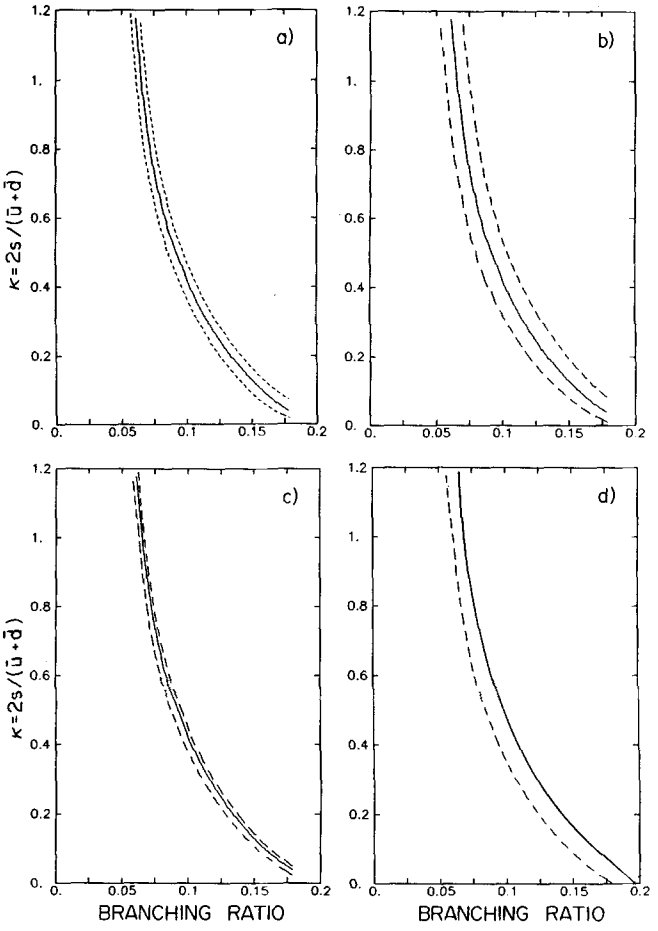

Fig. 15a–d. Correlation between the best fit for κ versus the semileptonic branching ratio (solid curve). In **a** the dashed curves show the effect of the 20% uncertainty in the background. In **b** the lower dashed curve shows the best fit with a charmed quark mass of 1.0 GeV/c^2 and the upper dashed curve with 1.9 GeV/c^2. In **c** the lower dashed curve shows the fit with the parameter ε in the Peterson fragmentation function set to 0.09 and the upper dashed curve with $\varepsilon = 0.29$. In **d** the dashed curve shows the fit with the fragmentation parameterized by a delta function at $Z = 0.68$

It is possible that a source of prompt like sign dimuons would also contribute to the opposite sign dimuon signal. To examine this effect, we have taken the charm-anticharm gluon bremsstrahlung model described earlier, and renormalized the rates by a factor of 42 to agree with the like sign dimuon prompt rate (as observed in this experiment). We have repeated the analysis after subtraction of this possible $c\bar{c}$ contamination. We find $\kappa = 0.41^{+0.13}_{-0.18} \pm 0.03$, indicating that possible enhanced $c\bar{c}$ production could add an additional systematic uncertainty of 0.02 to the determination of κ.

Table 11. Dependence of the fraction of the strange sea in the nucleon: $\kappa = 2s(x)/(\bar{u}(x)+\bar{d}(x))$ and $\eta_s = 2S/(U+D)$ for different charmed quark masses, m_c, and fragmentation functions. The variation in fragmentation function is parametrized by $\varepsilon = 0.09$, 0.19, and 0.29 in the Peterson et al. form and by a delta function $\delta(z-0.68)$ (last row). The first error shown includes the statistical error and the uncertainty in the charm branching ratio and the second error is due to the uncertainty in the level of the background

m_c	Fragmentation	κ	η_s
1.5	$\varepsilon=0.19$	$0.42^{+0.13}_{-0.10}\pm0.02$	$0.063^{+0.016}_{-0.013}\pm0.003$
1.0	$\varepsilon=0.19$	$0.35^{+0.11}_{-0.09}\pm0.02$	$0.054^{+0.014}_{-0.012}\pm0.003$
1.9	$\varepsilon=0.19$	$0.50^{+0.15}_{-0.12}\pm0.03$	$0.073^{+0.017}_{-0.013}\pm0.004$
1.5	$\varepsilon=0.09$	$0.41^{+0.12}_{-0.10}\pm0.02$	$0.061^{+0.015}_{-0.013}\pm0.003$
1.5	$\varepsilon=0.29$	$0.44^{+0.13}_{-0.11}\pm0.03$	$0.065^{+0.016}_{-0.014}\pm0.004$
1.5	$\delta(z-0.68)$	$0.39^{+0.12}_{-0.10}\pm0.02$	$0.059^{+0.015}_{-0.014}\pm0.003$

We have examined the energy dependence of κ by dividing the data into two energy bins above and below 100 GeV. The mean Q^2 of these energy bins are 10 GeV^2/c^2 and 27 GeV^2/c^2, respectively. The mean Q^2 for the sea antiquarks for these two energy bins is 9 (GeV/c)^2 and 23 (GeV/c)^2, respectively. The results of the fits for these two energy bins are shown in Table 12, along with the systematic effects of the uncertainty due to the charm quark mass and fragmentation. We find $\kappa = 0.19^{+0.18}_{-0.14}$ for $\langle E_\nu\rangle = 70$ GeV and $\kappa = 0.52^{+0.17}_{-0.15}$ for $\langle E_\nu\rangle = 180$ GeV, where the error includes uncertainties due to statistics, π and K background subtraction, charm quark mass and fragmentation. The errors in the two measurements of κ reported here are correlated due to common background level, charm quark mass and fragmentation assumptions. Therefore the ratio of κ in the high to low energy bins of 2.7 ± 1.0 has a reduced error. QCD calculations [29] predict less than a 10% increase in κ in the Q^2 range of this experiment from 9 to 23 GeV^2/c^2. The CDHS collaboration [24] reports $\kappa = 0.52\pm0.09$ and $(\bar{U}+\bar{D})/(U+D) = 0.13\pm0.02$ yielding $\eta_s = 0.068\pm0.016$ for $E_\nu > 35$ GeV independent of branching ratio. Their data are consistent with no energy dependence of κ, but are within the errors in the energy dependence found by this experiment.

Table 12a. Dependence of the fraction of the strange sea in the nucleon: $\kappa = 2s(x)/(\bar{u}(x)+\bar{d}(x))$ and $\eta_s = 2S/(U+D)$ extracted from low energy events with $30 < E_\nu < 100$ GeV for different charmed quark masses, m_c, and fragmentation functions. The variation in fragmentation function is parametrized by $\varepsilon = 0.09$, 0.19, and 0.29 in the Peterson et al. form and by a delta function $\delta(z-0.68)$ (last row). The errors are as in Table 11

m_c	Fragmentation	κ	η_s
1.5	$\varepsilon=0.19$	$0.19^{+0.13}_{-0.11}\pm0.04$	$0.031^{+0.019}_{-0.017}\pm0.006$
1.0	$\varepsilon=0.19$	$0.12^{+0.10}_{-0.08}\pm0.02$	$0.020^{+0.015}_{-0.013}\pm0.003$
1.9	$\varepsilon=0.19$	$0.30^{+0.15}_{-0.12}\pm0.04$	$0.047^{+0.020}_{-0.017}\pm0.006$
1.5	$\varepsilon=0.09$	$0.15^{+0.13}_{-0.11}\pm0.05$	$0.025^{+0.019}_{-0.018}\pm0.008$
1.5	$\varepsilon=0.29$	$0.24^{+0.13}_{-0.11}\pm0.04$	$0.038^{+0.018}_{-0.017}\pm0.006$
1.5	$\delta(z-0.68)$	$0.14^{+0.12}_{-0.10}\pm0.04$	$0.023^{+0.018}_{-0.016}\pm0.006$

Table 12b. Dependence of the fraction of the strange sea in the nucleon for high energy events with $100 < E_\nu < 230$ GeV as in **12a**

m_c	Fragmentation	κ	η_s
1.5	$\varepsilon=0.19$	$0.52^{+0.16}_{-0.12}\pm0.03$	$0.075^{+0.018}_{-0.015}\pm0.004$
1.0	$\varepsilon=0.19$	$0.45^{+0.14}_{-0.11}\pm0.03$	$0.066^{+0.017}_{-0.014}\pm0.004$
1.9	$\varepsilon=0.19$	$0.59^{+0.19}_{-0.14}\pm0.04$	$0.083^{+0.020}_{-0.017}\pm0.005$
1.5	$\varepsilon=0.09$	$0.50^{+0.15}_{-0.12}\pm0.03$	$0.071^{+0.018}_{-0.015}\pm0.004$
1.5	$\varepsilon=0.29$	$0.53^{+0.16}_{-0.12}\pm0.03$	$0.076^{+0.018}_{-0.015}\pm0.004$
1.5	$\delta(z-0.68)$	$0.49^{+0.15}_{-0.12}\pm0.03$	$0.071^{+0.017}_{-0.015}\pm0.004$

Figure 16 shows for the two energy bins the agreement between the observed neutrino-induced x distributions (after background subtraction) and the charm Monte Carlo prediction using the fitted values of κ. These values of κ correspond to $\eta_s = 0.031^{+0.025}_{-0.022}$ for $30 < E_\nu < 100$ GeV and $\eta_s = 0.075\pm0.019$ for $100 < E_\nu < 230$ GeV. The 1, 2 and 3 σ contours on the χ^2 surface as a function of κ and charm branching ratio are shown for the two energy bins in Fig. 17. Figures 18a and c show the best fit values for the energy regions $30 < E_\nu < 100$ GeV and $100 < E_\nu < 230$ GeV, respectively. Figures 18b and d show the best fit values of κ for the two energy regions with $m_c = 1.0$, 1.5 and 1.9 GeV/c^2. While the data are not compelling, these data and the CDHS [24] data are consistent with some rise in the value of κ with energy.

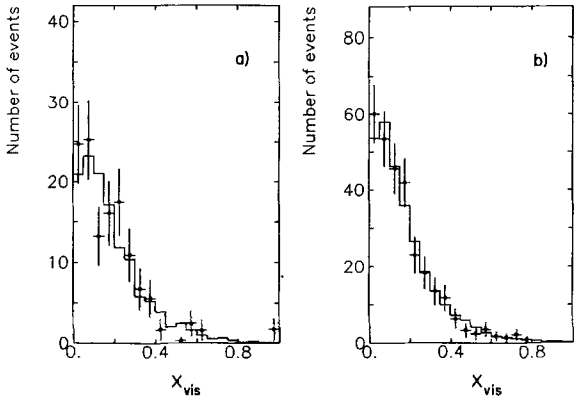

Fig. 16a, b. Bjorken x distributions of opposite sign background subtracted dimuon data with $P_\mu > 4.3$ GeV/c (points with error bars) and the single charm Monte Carlo (solid line) for $30 < E_\nu < 100$ GeV **a** and $100 < E_\nu < 230$ GeV **b**

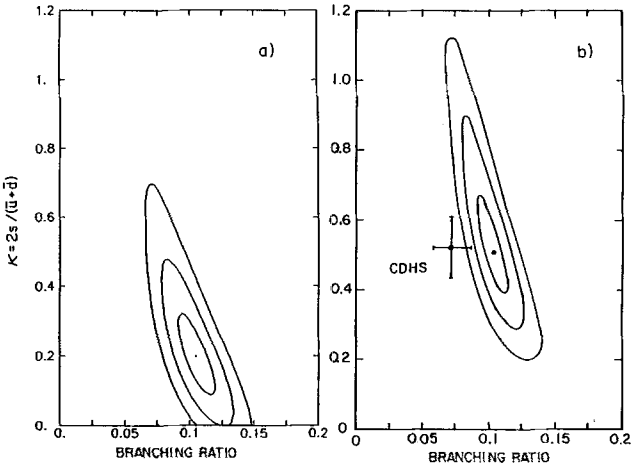

Fig. 17a, b. χ^2 contours as a function of κ and charm semileptonic branching ratio from fits to the ν and $\bar{\nu}$ x distributions. **a** is for $30 < E_\nu < 100$ GeV and **b** is for $100 < E_\nu < 230$ GeV. Shown are the 1, 2, and 3 standard deviation contours for $\varepsilon = 0.19$ and $m_c = 1.5$ GeV/c^2. The charm semileptonic branching ratio is constrained to be consistent with the value of 0.109 ± 0.014. Also shown on **b** is the value of the CDHS WBB measurement [24] for $E_\nu > 35$ GeV

A possible explanation for observing an energy dependence of κ in our data is an energy dependent charm semileptonic branching ratio. Such is the case if there is an increased relative percentage of Λ_c production at low energy [18] since the Λ_c semileptonic branching ratio is about 4%. The charm Monte Carlo model includes only charged and neutral D meson production, which has a higher average semileptonic semileptonic branching ratio of about 11%. It should be noted that the CDHS [24] extraction of κ is not dependent on the charm semileptonic branching ratio.

Another possibility is that there exists at high energy an additional source of opposite sign dimuons.

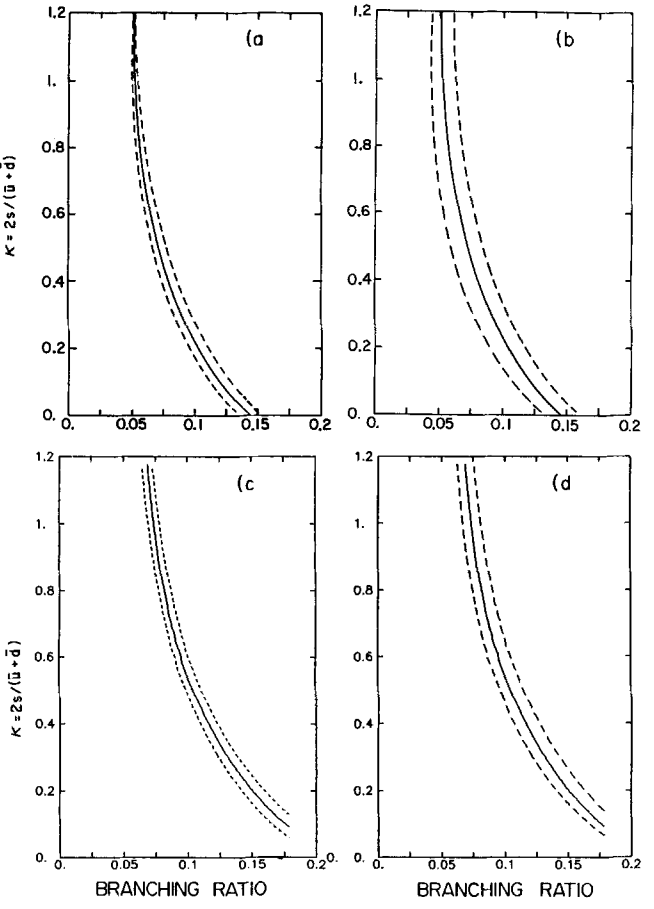

Fig. 18a–d. Correlation between the best fit for κ versus the semileptonic branching ratio (solid curve) for two energy ranges. **a** and **b** are for $30 < E_\nu < 100$ GeV while **c** and **d** are for $100 < E_\nu < 230$ GeV. In **a** and **c** the dashed curves show the effect of the 20% uncertainty in the background. In **b** and **d**, the lower dashed curve shows the best fit with a charm quark mass of 1.0 GeV/c^2 and the upper dashed curve with 1.9 GeV/c^2

An example would be the $c\bar{c}$ gluon bremsstrahlung model previously described where the c quark decays into a μ^+. To test this hypothesis, as in the case of the like sign dimuon analysis, we added 42 times the rate of $c\bar{c}$ production calculated in first order QCD [13] to the π and K decay background subtraction. We find only a small change in the K values shown in Table 13: $\kappa = 0.20^{+0.13}_{-0.10} \pm 0.04$ for $\langle E_\nu \rangle = 70$ GeV and $\kappa = 0.49^{+0.16}_{-0.12} \pm 0.04$ for $\langle E_\nu \rangle = 180$ GeV, where the first error includes the statistical error and the uncertainty in the charm branching ratio, and the second error is due to the uncertainty in the level of the background.

Observation of an energy dependence of κ would also be caused by a threshold behavior of neutrino-charm production which may not be properly described by slow rescaling. The rates in Fig. 10 suggest

Table 13. Effect of a $c-\bar{c}$ contamination (at a rate 42 times larger than the first order QCD) in the opposite-sign dimuon production on the determination of the parameter κ. The first error is statistical, the second is the systematic error due to the $\pm 20\%$ background uncertainty. The energy and four-momentum transfer are the means of the measured values of the dimuon events. The errors are as in Table 11

Energy (GeV)	$\langle E_\nu \rangle$ (GeV)	$\langle Q^2 \rangle$ (GeV^2/c^2)	κ	η_s
30–100	69	10	$0.20^{+0.13}_{-0.10}\pm 0.04$	$0.032^{+0.019}_{-0.016}\pm 0.006$
100–230	181	27	$0.49^{+0.18}_{-0.12}\pm 0.04$	$0.071^{+0.021}_{-0.015}\pm 0.005$
30–230	147	18	$0.41^{+0.13}_{-0.10}\pm 0.03$	$0.061^{+0.016}_{-0.013}\pm 0.004$

that slow rescaling with $m_c = 1.9$ GeV/c^2 is favored over $m_c = 1.5$ GeV/c^2 if this were the only mechanism. A repeated analysis with $m_c = 1.9$ GeV/c^2 (see Table 12) yields $\kappa = 0.30^{+0.15}_{-0.12} \pm 0.04$ for $\langle E_\nu \rangle = 70$ GeV and $\kappa = 0.59^{+0.19}_{-0.14} \pm 0.04$ for $\langle E_\nu \rangle = 180$ GeV, where the errors are defined as above.

The studies above indicate that at higher neutrino energies the extraction of κ is less sensitive to assumptions about the charmed quark mass and the charm semileptonic branching ratio.

Conclusions

The 18 observed like sign dimuon events with $P_\mu > 9$ GeV/c yield 6.6 ± 4.8 prompt events after background subtraction. This yields an average acceptance corrected rate for prompt like sign muon production of $(1.0 \pm 0.7) \times 10^{-4}$ per single muon event. Most distributions of the kinematic variables of the like sign dimuon events are similar to those expected from the hadronic shower background.

The observed rates and kinematic distributions of the prompt opposite sign dimuon signal are consistent with single charm production. The fully corrected rate with respect to single muon events reaches $(9.0 \pm 1.1) \times 10^{-3}$ at $E_\nu = 204$ GeV. If, in addition, we correct for slow rescaling with $m_c = 1.5$ GeV/c^2, we obtain a rate of $(11.1 \pm 1.4) \times 10^{-3}$. These data are used to extract a value for the fraction of the strange sea in the nucleon, $\kappa = 2\, s/(\bar{u}+\bar{d}) = 0.42^{+0.15}_{-0.13}$ corresponding to $\eta_s = 2\, s/(u+d) = 0.063^{+0.18}_{-0.17}$. The value of κ is found to have a possible energy dependence with $\kappa = 0.19^{+0.18}_{-0.14}$ at $\langle E_\nu \rangle = 70$ GeV ($\langle Q^2 \rangle = 9$ GeV^2/c^2) and $0.52^{+0.17}_{-0.15}$ at $\langle E_\nu \rangle = 180$ GeV ($\langle Q^2 \rangle = 23$ GeV^2/c^2). However, the observed energy dependence of κ may not be due to a Q^2 dependence of the strange sea (which is expected to be less than 10%), but to either charmed quark threshold or branching ratio effects (a larger fraction of Λ_c's near threshold) at low energy. Because of the uncertainties at low energy, we quote a value for κ using only the $E_\nu > 100$ GeV data. At these energies we determine $\kappa = 0.52^{+0.17}_{-0.15}$ and $\eta_s = 0.075 \pm 0.019$ at a $\langle Q^2 \rangle_{\text{sea}} = 23$ GeV^2/c^2.

Appendix A: Pion/Kaon Decay Background

A.1. Introduction

The principal source of background for dimuon events is muon production by pions and kaons in the hadron shower. In a high density calorimeter, most of the pions and kaons interact before decaying. Non-prompt muons come from two sources: (1) muonic decays of pions and kaons produced in primary neutrino interactions; and (2) muon production in subsequent interactions of the primary hadrons (pions, kaons, and protons) in the calorimeter either from secondary π and K decays or from hadronic charmed particle production. The muon production in the hadronic shower cascade is difficult to model accurately. We have therefore chosen to use experimental measurements of muon production by incident pions for this component and assumed that these measurements also characterize muon production by other hadrons.

In order to calculate the non-prompt background, two pieces of experimental information are needed: (1) the multiplicity and energy distribution of hadrons produced in the neutrino-iron ($\nu-$Fe) interactions, expressed in terms of fragmentation functions; and (2) the probability of muon production by hadrons interacting in the neutrino target/calorimeter. These two topics are discussed in the next two sections.

A.2. Hadron Production in Neutrino-Iron Interactions

The individual fragmentation functions are obtained from the Lund Monte Carlo program [3]. The Lund program provides a good description of many sets of experimental data [30, 31]. Fragmentation functions ($D(Z)$) from this program are in good agreement

with measured values for most reactions over a wide range of $Z = E_h/E_T$, the fraction of the total hadron energy, E_T, carried by a hadron h with energy E_h. However, the predicted values of $D(Z)$ are somewhat higher than measured for $Z > 0.5$ [32].

The Lund model was used with its default parameters except for two modifications as recently suggested (see Refs. 32, 33). The minimum energy, $E_{\min}$, above which a quark-antiquark pair is created was set to 0.2 GeV instead of the default 1.1 GeV. The strangeness suppression parameter, λ, which is the ratio of the probability of producing an $s\bar{s}$ pair to the probability of producing a $u\bar{u}$ or $d\bar{d}$ pair in the fragmentation chain, was set to 0.2 instead of the default of 0.3. The effects of setting $E_{\min} = 1.1$, $\lambda = 0.1$, and $\lambda = 0.3$ were studied and included in the estimate of the systematic error in the background calculation.

The Lund Monte Carlo program was directly checked against hadron fragmentation functions derived from experimental data. For the purposes of this comparison, two sources of data are used to obtain the individual hadron fragmentation functions. First, data from the BEBC collaboration [4] for neutrinos interacting in neon are used to obtain fits to the fragmentation functions for all positive and all negative hadrons. Second, the fragmentation functions for individual hadron species were extracted by combining these fits with the relative production ratios measured by the EMC collaboration [30] for $\mu - p$ interactions. In the forward hemisphere ($Z > 0.1$) $\mu - p$ and $\nu - p$ interactions should be similar, since both are dominated by u quark fragmentation. The data are fit to functions of Z [8] and yield the relative rates of pions, kaons, and protons integrated over W^2 from 16 to 400 GeV^2/c^4 (average $W^2 = 130$ GeV^2/c^4). The neutral kaon multiplicities are taken to be the average of the K^+ and K^- values and neutron/antineutron production rates are assumed to be the same as proton/antiproton rates. This fitting procedure has inherent systematic errors due to the assumptions involved. First, $\nu - \mathrm{Ne}$ and $\mu - p$ interactions are used instead of $\nu - \mathrm{Fe}$ interactions. Second, the relative EMC production fractions are assumed to be independent of W^2. For these reasons we have used these results only as a consistency test on the Lund fragmentation functions.

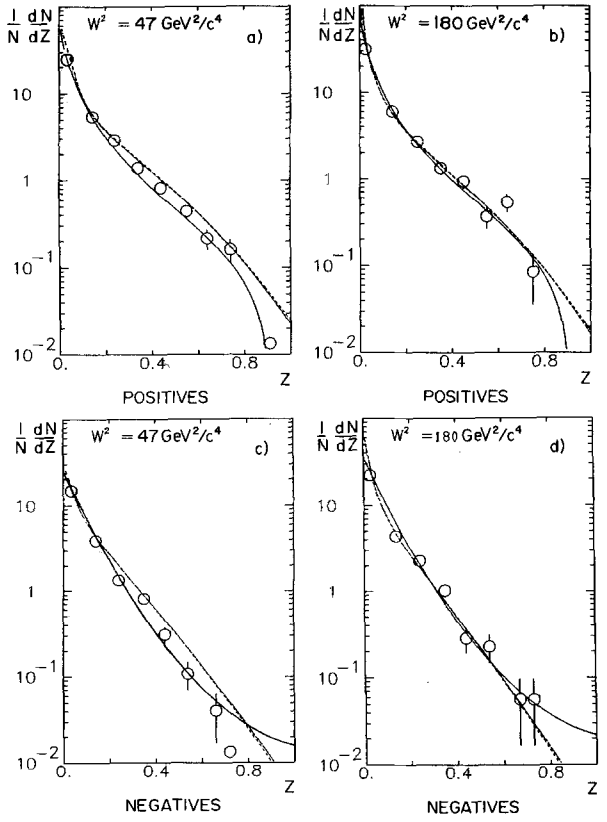

Fig. 19a–d. Positive and negative fragmentation functions from BEBC [4]. The solid line shows the fit to these data; dashed-dotted lines represent functions obtained with the Lund Monte Carlo with $\lambda = 0.1$, 0.2, and 0.3

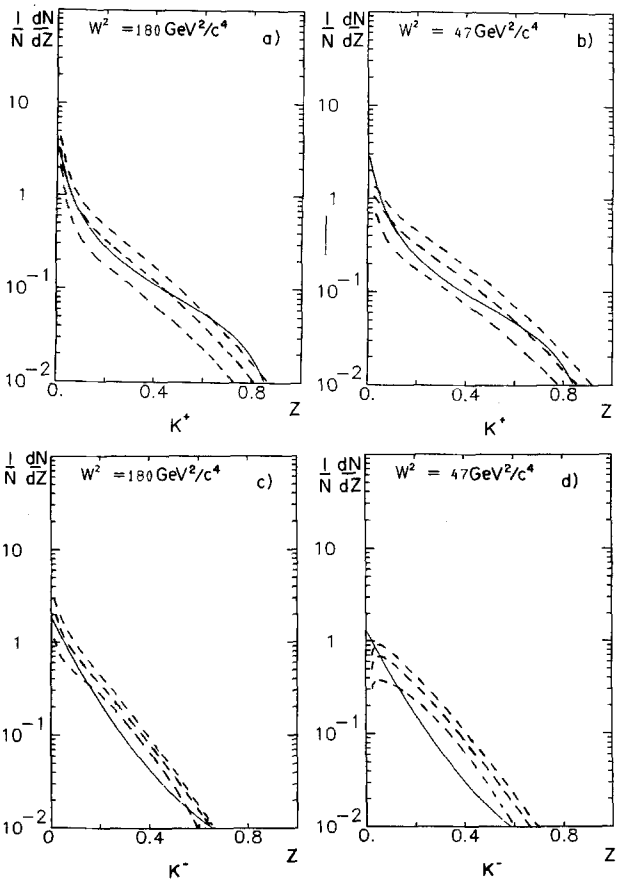

Fig. 20a–d. K^+ and K^- fragmentation functions from the fits to BEBC [4] and EMC [5] data (solid line) and from the Lund Monte Carlo (dashed-dotted lines: the top line is with $\lambda = 0.3$, the middle with $\lambda = 0.2$ and the bottom with $\lambda = 0.1$)

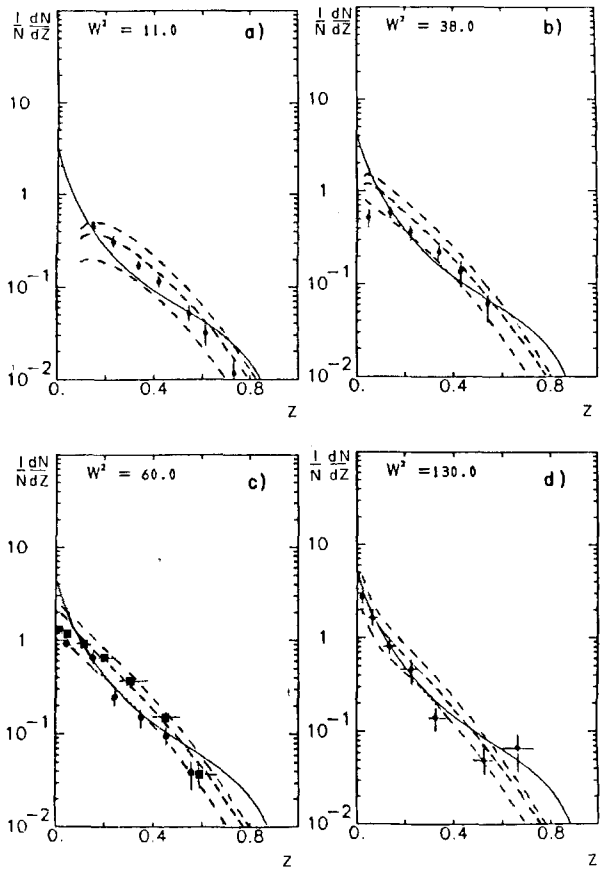

Fig. 21a–d. K^+ and K^- fragmentation functions from the fits to BEBC [4] and EMC [5] data (solid line) and from the Lund Monte Carlo (dashed-dotted lines: the top line is with $\lambda=0.3$, the middle with $\lambda=0.2$, and the bottom with $\lambda=0.1$). The data points are from [34a] in **a**, [34b] in **b**, [4] in **c**, and [34c] in **d**

Fragmentation functions obtained from BEBC/EMC data are compared to the above fits and to the Lund Monte Carlo predictions in Fig. 19. Figure 20 shows charged kaon fragmentation functions obtained from BEBC/EMC data and compared to the Lund Monte Carlo predictions with three values of the parameter $\lambda=0.1$, 0.2 and 0.3. Figure 21 shows K^0 fragmentation functions obtained from the BEBC/EMC data and compared to the Lund Monte Carlo prediction with $\lambda=0.1$, 0.2 and 0.3 along with measurements from four other bubble chamber experiments [4, 34] at corresponding values of W^2.

A.3. Muon Production in Hadron Interactions in Iron

Muon production from pion interactions in a variable density, totally absorbing iron calorimeter has been measured in Fermilab experiments E379 and E595 [6]. The experiments measured the rate of muon production ρ_{shower} (p_{cut}, E_h) for five muon momentum cuts (p_{cut}), $P_\mu > 4.3$, 8.45, 9.45, and 15.45 and 20.45 GeV/c, in showers initiated by an incident π^- beam with energies E_h of 40, 75, 150, and 225 GeV. Determination of positive and negative muon production was possible at all but the lowest P_{cut} of 4.3 GeV/c. Data were taken at two calorimeter average densities (6.12 g/cm^3 and 3.06 g/cm^3), allowing interpolation to the average density of our neutrino target/calorimeter (4.27 g/cm^3). The rates are presented in Table 14 along with the statistical errors. (A systematic error of $\pm 20\%$, not shown in the table, should also be included to account for acceptance uncertainties.) The energy loss part of the muon momentum calculation uses the assumption that all muons are produced at the front of the calorimeter; this is the appropriate method for calculating backgrounds for the dimuon measurements.

These muon production rates are then interpolated to the proper density of the neutrino target and, in addition, extrapolated to energies below 40 GeV. This extrapolation is accomplished using a Lund Monte Carlo calculation under the assumption that neutrino and pion induced final states are similar. Figure 22 shows power law fits to the data along with this extrapolation below 40 GeV. It is further assumed that rates for μ^- and μ^+ production in a π^- beam are the same as the corresponding μ^+ and μ^- rates in a π^+ beam. The muon yields from showers initiated by kaons, protons and neutrons were obtained by correcting the yields from pion initiated showers, using the results from [6] and [35]. These factors are described in [8] and averaged 1.8, 0.39 and 0.78 for kaons, protons and neutrons, respectively. Due to the fact that hadron showers may produce muons in pairs and, when both muons are observed, such events do not contribute to the dimuon background, there is a correction of 0.9 that multiplies the total secondary shower yield. These corrections together result in a 3% decrease in the total muon yield as compared to the case where the yields from all secondary particles are assumed to equal that from pions, and pair production is ignored.

A.4. Background Calculation

The calculation of the non-prompt background is made using the information of the preceding two sections. The contribution from the decay of a primary hadron (h) is calculated as follows, the probability

$$\pi^{\text{Decay}}(P_{\text{cut}}, \nu, x) = \sum_{\substack{\text{hadron} \\ \text{types}}} \int_0^1 D^h(Z, W^2)\, \rho_{\text{decay}}(P'_{\text{cut}}, E'_h)\, dz$$

Table 14. μ^+ and μ^- rates from Fermilab experiment E379 for five muon momentum cuts and four energies of the π^- beam at two different target densities. The errors are shown in parentheses

Energy: (GeV)		40		75		150		225	
Density: (g/cm^3)		6.21	3.06	6.21	3.06	6.21	3.06	6.21	3.06
P_μ Cut (GeV/c)	Rate								
4.3	$(\mu^+ + \mu^-)$ $\times 10^{-3}$	0.900 (0.060)	1.390 (0.080)	1.924 (0.070)	3.210 (0.150)	4.220 (0.170)	7.030 (0.290)	6.340 (0.270)	11.070 (0.480)
8.45	μ^+ $\times 10^{-3}$	0.088 (0.012)	0.127 (0.019)	0.234 (0.021)	0.366 (0.044)	0.487 (0.056)	1.149 (0.111)	0.939 (0.101)	1.523 (0.161)
	μ^- $\times 10^{-3}$	0.115 (0.014)	0.179 (0.023)	0.247 (0.022)	0.451 (0.049)	0.547 (0.060)	0.915 (0.099)	0.777 (0.092)	1.574 (0.164)
9.45	μ^+ $\times 10^{-3}$	0.077 (0.012)	0.095 (0.017)	0.208 (0.020)	0.313 (0.041)	0.378 (0.050)	0.904 (0.098)	0.734 (0.089)	1.198 (0.143)
	μ^- $\times 10^{-3}$	0.062 (0.015)	0.133 (0.020)	0.146 (0.016)	0.260 (0.037)	0.384 (0.050)	0.585 (0.079)	0.561 (0.078)	0.941 (0.127)
15.45	μ^+ $\times 10^{-4}$	0.120 (0.045)	0.202 (0.080)	0.806 (0.123)	0.954 (0.225)	1.433 (0.306)	2.979 (0.563)	3.668 (0.629)	3.422 (0.765)
	μ^- $\times 10^{-4}$	– –	– –	0.581 (0.104)	1.114 (0.243)	1.433 (0.306)	1.809 (0.439)	3.237 (0.591)	4.790 (0.905)
20.45	μ^+ $\times 10^{-4}$	– –	– –	0.337 (0.077)	0.636 (0.184)	0.717 (0.216)	1.383 (0.384)	1.942 (0.458)	1.882 (0.567)
	μ^- $\times 10^{-4}$	– –	– –	0.112 (0.046)	0.265 (0.119)	0.717 (0.216)	1.170 (0.353)	2.266 (0.494)	3.422 (0.765)

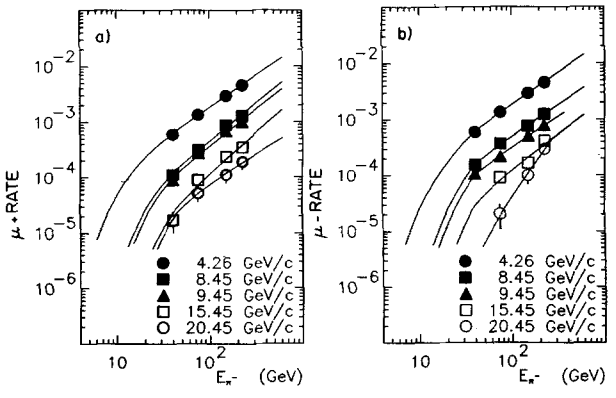

Fig. 22a, b. The points are the measurements for μ^- and μ^+ rates from Fermilab experiment E379 at five muon momentum cuts. Solid lines show the fit used in the background calculation

where $W^2 = 2Mv(1-x)+M^2$, $E'_h = Zv - \Delta$ and $P'_{\text{cut}} = P_{\text{cut}} - \Delta$.
(Δ is 0.29 and 0.32 GeV for pions and kaons respectively and corrects for the energy loss of the hadron because the average hadron decay point is one interaction length downstream of the neutrino event vertex.)

The function $\rho_{\text{decay}}(P_{\text{cut}}, E_h)$ describes the probability for a π or K decay to produce a muon greater than P_{cut} and is given by:

$$\rho_{\text{decay}}(P_{\text{cut}}, E_h) = \begin{cases} 0 & \text{for } E_h < P_{\text{cut}} \\ \dfrac{r_h(1-P_{\text{cut}}/E_h)}{1-R_h} & \text{for } P_{\text{cut}} < E_h < P_{\text{cut}}/R_h \\ r_h & \text{for } E_h > P_{\text{cut}}/R_h \end{cases}$$

where $R_h = \dfrac{m_\mu^2}{m_h^2}$ and $r_h = \dfrac{\lambda^h_{\text{decay length}}}{\lambda^h_{\text{interaction length}}}$.

Using the measurements of [36], we find the interaction length, $\lambda^h_{\text{interaction length}}$, for an iron target with a density of 4.27 g/cm^3 ($\lambda_{\text{int}} = 1.764\ \lambda^{\text{Fe}}_{\text{int}}$) is:

$$\lambda(\pi^\pm) = \begin{cases} 35.69 \text{ cm} & P_\pi > 22 \text{ GeV/c} \\ 2.085 \times 10^4/(678.0 - 4.2\, P_\pi(\text{GeV/c})) \text{ cm} & \text{for } P_\pi \leqq 22 \text{ GeV/c} \end{cases}$$

$$\lambda(K^+) = 40.94 \text{ cm}$$

$$\lambda(K^-) = 39.48 \text{ cm}.$$

In the calculation, both $K^\pm \to \mu^\pm \nu$ and $K^\pm \to \pi^\pm \pi^0$ with the $\pi^\pm \to \mu^\pm \nu$ are included.

The muon rate from the primary hadron interactions is calculated by convoluting the fragmentation

functions of Sect. A.2 with the production rates given in Sect. A.3.

$$\pi^{\text{shower}}(P_{\text{cut}}, \nu, x) = \sum_{\substack{\text{hadron} \\ \text{types}}} \int_0^1 D^h(Z, W^2)\, \rho_{\text{shower}}(P_{\text{cut}}, E_h)\, \mathrm{d}z.$$

The total muon production probability is then the sum of the two parts:

$$\pi^{\text{Total}}(P_{\text{cut}}, \nu, x) = \pi^{\text{Decay}}(P_{\text{cut}}, \nu, x) + \pi^{\text{Shower}}(P_{\text{cut}}, \nu, x)$$

and is given as a function of muon momentum cut, $P_{\mu\,\text{cut}}$, x, and ν (Fig. 23). A calculation of the background for the neutrino data sample is obtained by convoluting this total probability with the observed charged current events.

We have estimated the total systematic error inherent in these procedures. The Lund Monte Carlo fragmentation functions are generated for ν-(free nucleon) interactions. It was assumed that they are the same for ν–Fe interactions. The EMC measurements of fragmentation functions for various nuclear targets [37] indicate that this leads to an uncertainty of $\pm 15\%$ due to possible nuclear effects. A change of the λ parameter in the Lund Monte Carlo from 0.2 to 0.3 or 0.1 leads to a 6% change. The $\pm 20\%$ uncertainty in the contribution of secondary hadrons leads to a $\pm 10\%$ uncertainty. The parametrizations of the fragmentation functions and final muon rates were obtained with a $\pm 5\%$ precision that leads to a $\pm 5\%$ background error. The total systematic error of $\pm 20\%$ is obtained by combining these errors in quadrature.

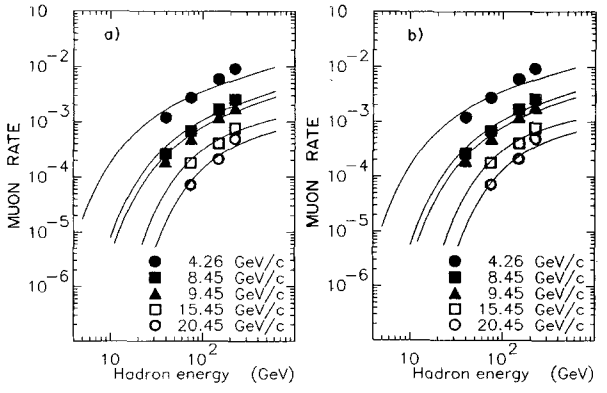

Fig. 23a, b. Total muon rates as a function of hadron energy as measured by Fermilab experiment E379 for five muon momentum cuts (data points). The curves represent the neutrino and antineutrino hadron shower induced total muon rates obtained by the background calculation at $x_{BJ}=0.2$

Appendix B: Charmed Semileptonic Decay

The kinematics of the prompt muons from charm decay were modeled as if they all came from the decay of D mesons. The small amount of Λ_c production does not change the kinematics significantly. However, we did include the presence of Λ_c production in the calculation of the charm branching ratio to muons.

The kinematics of the semileptonic charmed decay were modeled using the squared matrix element for $D \to K^* \mu \nu$ [38]:

$$|M|^2 = (2 p_D p_\nu)(2 p_D p_\mu) - (M_D^2 - 2 M_x^2)(2 p_\nu p_\mu).$$

The mass M_x was a free parameter chosen [20a] to be 0.65 GeV/c^2 to provide a reasonable fit to the inclusive D decay electron energy spectrum measured at the $\psi''(3770)$ by the DELCO group at SLAC [25a].

The semileptonic branching ratio for the specific mixture of charm particles produced in neutrino interactions has not been directly measured. However, it can be determined by combining data on branching ratios of charm particles into leptons from $e^+ e^-$ reactions with information about the composition of charm particles produced in neutrino reactions as measured in neutrino emulsion data.

Fermilab experiment E531 observed a total of 25 charmed particles produced in neutrino interactions with visible energy $E_\nu > 30$ GeV in their hybrid emulsion spectrometer [18]. Of these, there are 12 neutral charmed mesons (D^0 and $\bar{D}_0$), 10 D^+ and 3 charmed hyperons, 2 of which are identified as Λ_c^+.

In addition, the Mark III collaboration at SLAC [23] reports the following branching ratios:

$$B(D^+ \to e^+ X) = 17.0 \pm 1.9 \pm 0.7\%,$$

$$B(D^0 \to e^+ X) = 7.5 \pm 1.1 \pm 0.4\%.$$

The Λ_c branching ratio to electrons must be determined from the D meson branching ratios and the lifetimes of the D and Λ_c. The lifetimes are measured [39] to be:

$$\tau_{D^+} = 9.3^{+2.7}_{-1.8} \times 10^{-13},$$

$$\tau_{D^0} = 4.0^{+1.2}_{-1.9} \times 10^{-13},$$

$$\tau_{\Lambda_c} = 2.2^{+0.9}_{-0.5} \times 10^{-13}.$$

The calculated Λ_c branching ratio to electrons is 4.1 $\pm 2.1\%$. The inclusion of Λ_c production in the calculation of the neutrino branching ratio lowers it by 0.2%.

The combination of the individual charmed particle branching ratios with the composition of charmed particles found in neutrino interactions yields the electron branching ratio for neutrino charm production of:

$$B_e(\text{charm} \to eX) = 10.9 \pm 1.4\%.$$

In our analysis, it is assumed that the charm branching ratio into muons is equal to the charm branching ratio into electrons.

References

1. R. Blair et al.: Phys. Rev. Lett. **51**, 3431 (1983)
2. R. Blair et al.: Nucl. Instrum. Methods **226**, 281 (1984)
3. T. Sjostrand: Comput. Phys. Commun. **27**, 243 (1982)
4. P.C. Bosetti et al.: Nucl. Phys. **B149**, 13 (1979); **B209**, 29 (1982)
5. J.J. Aubert et al.: Phys. Lett. **114B**, 373 (1982)
6. Fermilab E379/595 (c.f. J. Ritchie: Ph.D. Thesis, UR 861, University of Rochester (1983) and K.W.B. Merritt: Ph.D. Thesis, Caltech (1981).) Data do not exist for $E_\pi < 40$ GeV, where we use a MC calculation
7. F.W. Brasse: In: Proc. of XXth Int. Conf., Madison, Wisconsin, p. 755 (1980)
8. K. Lang: Ph.D. Thesis, University of Rochester, UR 908 (1985)
9. B. Young, T.F. Walsh, T.C. Yang: Phys. Lett. **74B**, 111 (1978); V. Barger, W.Y. Keung, R.J.N. Phillips: Phys. Rev. **D25**, 1803 (1982)
10. A. Bodek et al.: Phys. Lett. **113B**, 82 (1982)
11. J.G.H. deGroot et al.: Phys. Lett. **86B**, 103 (1979)
12. H. Burkhardt et al.: Z. Phys. C – Particles and Fields **31**, 39 (1986)
13. M. Jonker et al.: Phys. Lett. **107B**, 241 (1981)
14. T. Trinko et al.: Phys. Rev. **D23**, 1889 (1981)
15. K. Nishikawa et al.: Phys. Rev. Lett. **46**, 1555 (1981); Phys. Rev. Lett. **54**, 1336 (1985)
16. R.M. Godbole, D.P. Roy: Z. Phys. C – Particles and Fields **22**, 39 (1984)
17. C. Baltay et al.: Phys. Rev. Lett **41**, 73 (1978)
18. N. Ushida et al.: Phys. Lett. **121B**, 292 (1983)
19. R.M. Barnett: Phys. Rev. Lett. **36**, 1163 (1976); H. Georgi, H.D. Politzer: Phys. Rev. **D14**, 1829 (1976)
20a. B.J. Edwards, T.D. Gottschalk: Nucl. Phys. **B186**, 309 (1981); b. J. Kaplan, F. Martin: Nucl. Phys. **B115**, 333 (1976); C.H. Lai: Phys. Rev. **D18**, 1422 (1978). In the formulation of M. Kobayashi and K. Maskawa: Progr. Theor. Phys. **49**, 652 (1973), $\sin\theta_c$ is replaced by $\sin\theta_1 \cos\theta_2$ and $\cos\theta_c$ by $\cos\theta^1 \cos\theta_2 \cos\theta_3 - \sin\theta_2 \sin_3 e^{i\delta}$
21. D. MacFarlane et al.: Z. Phys. C – Particles and Fields **26**, 1 (1984)
22. M. Aguilar-Benitez et al.: Phys. Lett. **123B**, 103 (1983)
23. R.M. Baltrusaitis et al.: Phys. Rev. Lett. **54**, 1976 (1985)
24. H. Abramowicz et al.: Z. Phys. C – Particles and Fields **15**, 19 (1982)
25a. W. Bacino et al.: Phys. Rev. Lett. **43**, 1073 (1979); b. J.M. Feller et al.: Phys. Rev. Lett. **45**, 329 (1978); R.H. Shindler et al.: Phys. Rev. **24**, 78 (1981)
26. H. Albrecht et al.: Phys. Lett. **150B**, 235 (1985)
27. C. Peterson et al.: Phys. Rev. **D27**, 105 (1983)
28. J. Chapman: Proc. of the 12th SLAC Summer Institute on Particle Physics (1984)
29. E. Eichten et al.: Rev. Mod. Phys. **56**, 579 (1984); N.N. Nikolaev: U. of Tokyo preprint, INS Rep-539 (1985)
30. M. Arneodo et al.: Phys. Lett.**150B**, 458 (1985)
31. P. Allen et al.: Nucl. Phys. **B214**, 369 (1983); J.P. Albanese et al.: Phys. Lett.**144B**, 302 (1984); M. Arnedo et al.: Phys. Lett.**149B**, 415 (1984)
32. D. Allasia et al.: Z. Phys. C – Particles and Fields **24**, 119 (1984)
33. G.T. Jones et al.: Z. Phys. C – Particles and Fields **27**, 43 (1985)
34a. A.M. Cnops et al.: Proc. Rencontre de Moriond, France (1978); b. D. Allasia et al.: Nucl. Phys. **B224**, 1 (1984); c. M. Arneodo et al.: Phys. Lett.**145B**, 156 (1984); d. E. Wolin: Neutral Strange Particle Production in High Energy Neutrino Interactions, Ph.D. Thesis, U. of Washington, UTL-PUB-98 (1984)
35. A.E. Brenner et al.: Phys. Rev. **D26**, 1497 (1982)
36. S.P. Denisov et al.: Nucl. Phys. **B61**, 61 (1973); J.C. Allaby et al.: Sov. J. Nucl. Phys. **13**, 295 (1971)
37. A. Arvidson et al.: Nucl. Phys. **B246**, 381 (1984)
38. V. Barger, R.J.N. Phillips: Phys. Rev. **D14**, 80 (1976)
39. G. Kalmus: Proc. XXI Int. Conf. on High Energy Physics. Paris (1982)